

NASA TECHNICAL NOTE



NASA TN D-3650

NASA TN D-3650

C. 1

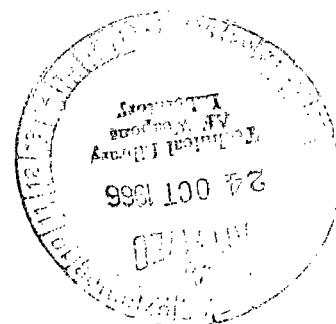
LOAN COPY: RETUI
AFWL (WLIL-2
KIRTLAND AFB, N



FEASIBILITY STUDY OF SECONDARY EMISSION ELECTRON MICROSCOPY FOR EXAMINING MATERIALS CONTAINING DISPERSED OXIDE PARTICLES

by L. Fredrick Norris and Walter S. Cremens

*Lewis Research Center
Cleveland, Ohio*



TECH LIBRARY KAFB, NM



0130257

NASA TN D-3650

FEASIBILITY STUDY OF SECONDARY EMISSION ELECTRON
MICROSCOPY FOR EXAMINING MATERIALS CONTAINING
DISPERSED OXIDE PARTICLES

By L. Fredrick Norris and Walter S. Cremens

Lewis Research Center
Cleveland, Ohio

NATIONAL AERONAUTICS AND SPACE ADMINISTRATION

For sale by the Clearinghouse for Federal Scientific and Technical Information
Springfield, Virginia 22151 - Price \$2.00

CONTENTS

	Page
SUMMARY	1
INTRODUCTION	2
SECONDARY EMISSION ELECTRON MICROSCOPY	3
APPARATUS, MATERIALS, AND PROCEDURES.	5
Description of Secondary Emission Electron Microscope (SEEM)	5
Operation of SEEM	7
Materials Examined	8
Specimen Preparation for SEEM Examination	10
Replication for Conventional Electron Microscopy	10
Particle Sizing and Counting	10
Determination of SEEM Resolution Limit	11
Experiments for Explanation of "Volume Percent Anomaly"	11
Investigation of Phase Discrimination.	11
RESULTS	12
Secondary Electron Emission Microscope	12
Particle Size and Particle Image Enlargement	18
Results of Experiments to Determine Ion Beam Penetration	30
Results of Investigation into Irregular Ion Beam Etching.	30
Phase Discrimination in Oxide/Oxide and Metal/Metal Systems	31
Other Practical Examples of Dispersion Microstructures Viewed by SEEM and by CEM	35
Nickel-base alloys.	35
Aluminum-base alloys	36
Tungsten-base alloys	36
DISCUSSION	42
Resolution and Detection Limits of SEEM.	42
Distortion - Preferential Enlargement of Oxide-Particle Images	43
Phase Discrimination	44
CONCLUSIONS	45
APPENDIX - QUALITATIVE EVIDENCE FOR IMAGE DISTORTION.	47
REFERENCES	48

FEASIBILITY STUDY OF SECONDARY EMISSION ELECTRON MICROSCOPY FOR EXAMINING MATERIALS CONTAINING DISPERSED OXIDE PARTICLES

by L. Fredrick Norris and Walter S. Cremens

Lewis Research Center

SUMMARY

The feasibility of using a secondary emission electron microscope (SEEM) to examine dispersion-strengthened materials was explored. Nickel, tungsten, and aluminum containing submicron oxide dispersoids were examined and the results compared with micrographs from a conventional electron microscope. Because secondary electron emission varies with chemical phase, separate phases, such as metal and oxide in a microstructure, can be differentiated because of different levels of brightness in the image.

A high metal/oxide contrast, desirable for quantitative metallography, was observed in most of the materials examined, but an unexpected preferential enlargement of oxide particle images was discovered, which precluded the anticipated use of the SEEM for measurement of microstructural parameters. The image enlargement gives rise to a detection limit of 350 \AA (0.035μ) for thoria particles in a nickel matrix, which value lies well below the measured resolution limit of 800 \AA (0.08μ).

Various levels of image brightness were also observed in a composite foil laminate of several metals. Phase discrimination between metals and between oxides was found to be limited to those combinations having substantially different yields of secondary electrons. However, discrimination between two different oxides in a metal matrix was not achieved under the various experimental conditions used.

For the specific purpose of examining ultrafine oxide dispersion microstructures, secondary emission electron microscopy does not provide important advantages over conventional electron microscopy. There are other applications, however, where the distortion associated with oxides may not limit the use of secondary emission microscopes.

INTRODUCTION

Electron microscopy has been traditionally employed in the examination of microstructures of dispersion-strengthened materials. This is a consequence of the inability of the light microscope to resolve dispersoid particles, which are usually well below 1 micron in diameter. However, electron microscopy replication techniques generally used for determining the distribution of the dispersoid in the matrix and quantitative microstructural parameters, such as volume percent dispersoid and interparticle spacing, also have certain shortcomings.

The conventional replication technique requires etching of a polished specimen to reveal phase differences. Small changes in etching procedure can have a marked effect on the apparent microstructure. Very fine dispersoid particles, for example, can be undercut and lost from the surface.

In a secondary emission electron microscope, unlike a conventional electron microscope (CEM), the surface of a specimen can be observed directly. The specimen is placed in the instrument column where it is bombarded with ions or electrons, which induce an emission of secondary electrons. The secondary electron image is then focused and magnified as in a CEM. Because the specimen itself is observed rather than a replica, the secondary emission electron microscope allows direct observation of the surface microstructure of materials over a wide range of temperatures and chemical environments. Furthermore, because the secondary emission yield varies with chemical phase, phase discrimination is possible without prior chemical etching of the specimen. Thus the use of secondary emission microscopy appeared to be an attractive companion technique to conventional electron microscopy.

To date, secondary emission microscopy has not been used for the examination of dispersion-strengthened materials. Most applications of a secondary emission electron microscope reported in the literature have involved microstructures containing only metallic phases. For example, various studies with Armco iron, aluminum, a uranium-molybdenum-aluminum alloy, and a pearlitic steel have been reviewed by Watts (ref. 1). Because a charging of the surface of nonconductors has a deleterious effect on the electron image, few investigators have examined ceramic materials. For such materials it has usually been necessary to deposit on the surface a thin layer, which has a low secondary electron yield and a relatively long mean free path for secondary electrons emitted from the substrate (ref. 2). Carbon has often been used for this purpose. By using a low-voltage (1.5 kV) incident-electron beam in a scanning secondary emission electron microscope, Thornly and Cartz (ref. 3) were able to view thorium and several alumina ceramics.

In preliminary experiments conducted at Lewis, various operational aspects of a commercial secondary emission electron microscope, hereinafter referred to as SEEM,

were investigated. Examination of a dispersion of coarse thoria particles in a tungsten matrix yielded micrographs characterized by extremely high oxide/matrix contrast. Specimens containing submicron oxide dispersoids in nickel also exhibited high contrast; however, quantitative metallography of micrographs of both materials revealed a major problem. It was found that the area fraction of oxide dispersoid observed in the micrographs was larger than the volume percent oxide known to be present in the sample. This "volume percent anomaly" necessarily became a subject of study since distorted values were obtained for microstructural parameters.

This study explored the possibilities of utilizing secondary emission electron microscopy for the examination of dispersion-strengthened materials. In particular, the feasibility of using the SEEM for determining quantitative microstructural parameters (particle size, volume percent dispersoid, interparticle spacing) was to be determined by examining dispersion-strengthened materials with particle sizes and interparticle spacings of less than 1 micron. Comparison could then be made between parameters determined by the SEEM and by a CEM. In addition, the sensitivity of phase discrimination was to be determined. An indication of whether the SEEM could be used to reveal the presence of additional metallic phases in a dispersion-strengthened alloy microstructure was also expected. The possibility of detecting contamination consisting of an oxide of the matrix in a metal/oxide dispersion product, that is, discriminating between two different oxide phases, was also to be determined.

Several dispersion-strengthened materials were examined in the SEEM and in a CEM under controlled conditions. These included three tungsten-thoria alloys, a nickel-thoria alloy (TD-Nickel), two nickel-alumina alloys, an aluminum-alumina alloy (Alcoa M-257), and a nickel - nickel oxide - alumina alloy. The last alloy and a multilayer foil laminate were used for part of the investigation of phase discrimination. The microstructures of tungsten-thoria and nickel-thoria alloys were utilized for quantitative metallography in solving the volume percent anomaly. Two unidirectionally solidified eutectics were also used, one in the measurement of the resolution limit of the SEEM, the other to reveal the ion-etching capabilities of the instrument.

SECONDARY EMISSION ELECTRON MICROSCOPY

The theory and practice of electron emission microscopy have been reviewed recently by Moellenstedt and Lenz (ref. 2). Emission microscopy is characterized by the emission of imaging electrons directly from the specimen-cathode. This is in contradistinction to reflection electron microscopy and electron mirror microscopy, wherein an external source of electrons is necessary (although the specimen itself is observed). The methods of inducing electron emission in emission microscopy include

photoemission, electron emission under ion, atom, or molecular bombardment, thermionic emission, and field emission.

The physics of secondary-electron emission has been treated by Bruining (ref. 4) and Kaminsky (ref. 5). The physical basis for secondary emission microscopy is the yield of secondary electrons, that is, the number of secondary electrons emitted per incident primary electron or ion. The yield is a function of the target material and its crystallographic orientation, the angle of incidence of the primary ion beam, the ion species, ion discharge potential, and, to some extent, the target temperature.

Two types of microscopes based on secondary electron emission have been developed. In one, a complete image of the cathode is formed at every instant on either a fluorescent screen or a photographic plate. A cone of ions sprayed onto the specimen by an ion gun induces the emission of secondary electrons, which is focused with a lens system. The instrument (SEEM) used in this study is an example.

In a second type, the specimen surface is scanned with a very small diameter electron beam. The secondary electrons emitted are used to control the intensity of a synchronized beam scanning a display tube. No lenses are used to focus the complete image. Scanning microscopes have recently been made available commercially by Cambridge Instrument Company, Ltd., of England and by Westinghouse Electric Instrument Corporation.

Both types of instruments have resolving powers intermediate between conventional electron microscopes and optical microscopes. The scanning secondary-emission microscopes have been reported by the manufacturers to have a resolving power (100 to 600 Å) somewhat superior to the SEEM (500 to 1000 Å). The depth of field of the scanning secondary-emission microscope is also greater than that of the SEEM; thus relatively irregular surfaces can be examined.

Microstructural details in micrographs obtained with a SEEM arise in two different ways. The differences in secondary emission yields from various chemical phases may be sufficient to permit discrimination between these phases by differences in their brightness levels. Secondly, surface structures present initially from prior etching or developed by ion etching during observation are revealed by their topography.

With a specimen consisting of two phases, such as a metal and its oxide, the differences in secondary electron emission between the phases, observed as differences in levels of brightness, allow these phases to be distinguished. The emission current from several metals of relevance to the present study are listed in table I (obtained from ref. 6) for different types of discharge ions. From such a tabulation it should be possible to choose the bombarding ion so that maximum separation of the phases can be effected in the specimen on the basis of image intensity.

Because the ion beam illuminates the specimen at shallow angles to the surface,

TABLE I. - EMISSION CURRENT IN NANOAMPERES FOR VARIOUS TARGET MATERIALS AND IONS

[Specimen temperature, 300° C; discharge current, 50μA; discharge voltage, 25 kV; data from ref. 6.]

Ions	Target material							
	Aluminum ^a	Zirconium	Carbon	Titanium	Tantalum	Tungsten	Nickel ^a	Gold
Hydrogen	160	100	40	38	28	24	25	25
Argon	57	66	28	23	17	13	11.5	7
Nitrogen	90	52	23	17.5	17	14	12	10.5
Oxygen	105	60	22	28	19	14	50	11
Air	90	54	24.5	20	18	15	17	10.5

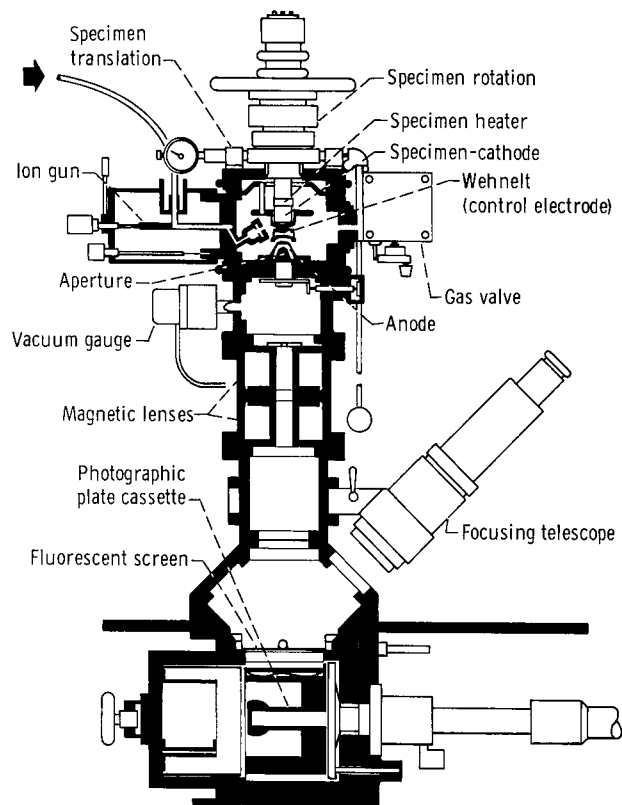
^aEmission enhanced by oxide layer.

topographical features of the surface are clearly revealed. At the highest angles (about 20°) the rough features of the surface are emphasized while at the lowest angles (about 2°) fine details become visible. Either high ion beam currents or long observation at low currents results in etching of the surface. Grain boundaries, deformation twins, and other surface features usually revealed in chemical etching are then displayed (ref. 1).

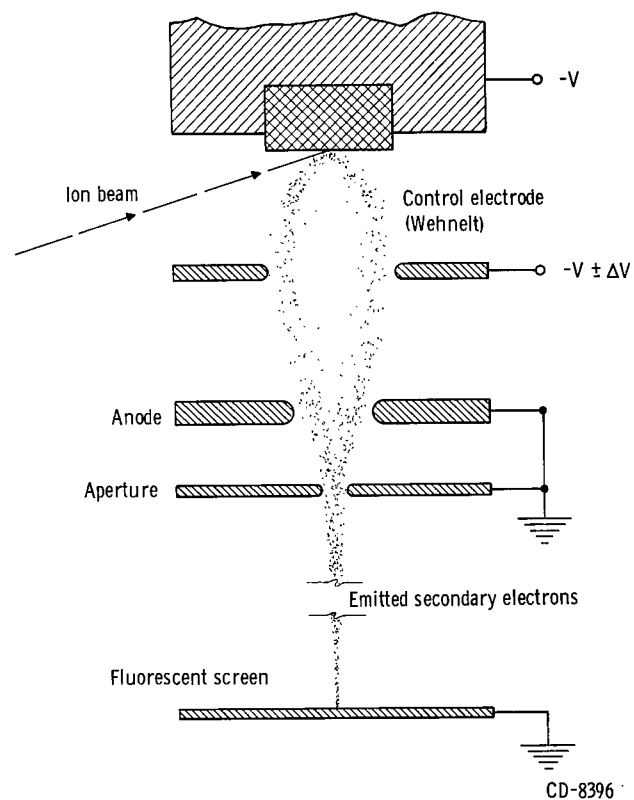
APPARATUS, MATERIALS, AND PROCEDURES

Description of Secondary Emission Electron Microscope (SEEM)

The secondary emission electron microscope used in this study is of the Moellenstedt-Dueker design and is commercially available from Balzers of Liechtenstein as the Metioscope (referred to as SEEM herein). A cross section through the vacuum column of the instrument is shown in figure 1(a). An inverted specimen, serving as the cathode, is bombarded by positive ions from the ion gun, which may be adjusted to various angles of impingement (2° to 20°). The secondary electrons emitted from the specimen are focused and accelerated by an electrostatic immersion objective consisting of the cathode, Wehnelt (direct-current control electrode), and anode. The image passes through an aperture and two magnetic lenses to the fluorescent screen or photographic plates for observation. A detailed schematic of the imaging components is given in figure 1(b). A telescope is used in final focusing. A tungsten wire resistance heater surrounding the specimen base allows heating to 1100° C. Temperature is measured by a thermocouple imbedded in the specimen base. The specimen head can be rotated or translated to change the area of the specimen viewed. Gases for a controlled chemical environment



(a) Sectional view of SEEM vacuum column.



(b) Detailed schematic of principal components in image-forming section.

Figure 1. - Sectional view of vacuum column and detailed schematic of image-forming section of secondary emission electron microscope (SEEM).

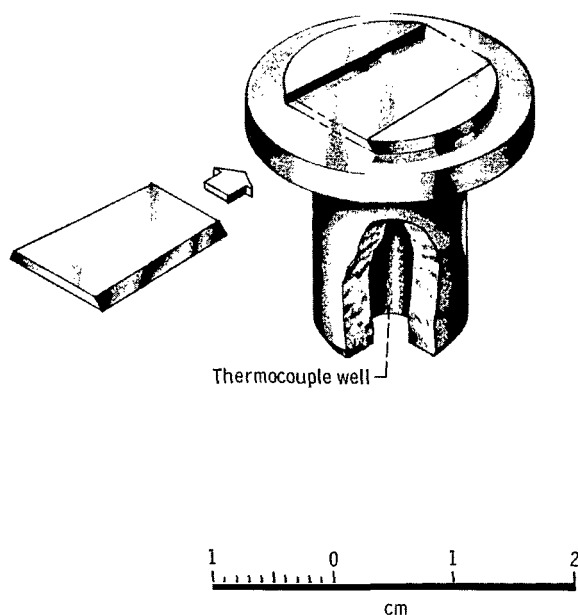


Figure 2. - Specimen holder and wedge-shaped specimen for SEEM.

can be admitted through a valve into the vacuum column.

Not shown in figure 1(a) is the vacuum pumping system. The column is evacuated by a two-stage rotary pump coupled with a baffled three-stage oil diffusion pump and liquid-nitrogen cold trap. The photographic plate cassette air lock is evacuated by a separate rotary pump. Column vacuum is measured by a cold-cathode gage.

For the present study, the SEEM specimen was modified to serve as a specimen holder, as shown in figure 2. The materials to be examined, generally in the shape of small pellets, were machined, mounted in these holders, and then polished.

Operation of SEEM

In common with conventional electron microscopes, the SEEM has basic operational features, such as evacuation of the column and alignment of the electron optics. With liquid nitrogen trapping, initial column pressures of 10^{-5} to 10^{-6} torr were achieved. During normal operation (with an ion beam current of $25 \mu\text{A}$), the column pressure was of the order of 2×10^{-4} torr.

Heating of the specimen was not generally necessary for the development of contrast between brightness levels of the metal and oxide phases. Exceptions were alloys containing thorium for which heating to the range of 400° to 500° C resulted in a marked increase in oxide/metal contrast over that at room temperature. However, most specimens in this study were run in the temperature range 50° to 500° C to reduce contamination by organic residues from sources such as diffusion pump oil. By outgassing at somewhat elevated temperatures, high voltage discharges, which contaminated the Wehnelt and anode, were minimized. Specimen heating rates of the order of 80° to 100° C per minute were employed.

Both the ion discharge potential and the ion beam current in the SEEM can be controlled over ranges of 9 to 18 kilovolts and 0 to 100 microamperes, respectively. In practice, the discharge potential is fixed for a given experiment, and the ion current is varied in the range 25 to 50 microamperes for general observation or to 100 microamperes

if ion etching and simultaneous observation are desired. With the higher ion currents, ion etching is accompanied by erosion of the specimen surface along the direction of the beam. To simplify interpretation of the microstructure, it is therefore important to make observations quickly and to use ion beam currents as low as practicable, usually about 25 microamperes. Undesirable erosion of the specimen surface can also be minimized by using a light gas (such as hydrogen or helium) in the ion source and by using low ion potentials.

Materials Examined

Materials examined in this study are listed in table II. The main subjects of examination were dispersion alloys with matrices of nickel, aluminum, and tungsten containing dispersions of thoria, alumina, or zirconia. Some all-metal composite materials, a foil laminate and two unidirectionally solidified eutectics, were included to illustrate particular points.

The most intensive study was done on TD-Nickel, nickel containing a fine dispersion of thoria, with a particle size range which was known to bracket the suspected resolution of the SEEM. The particular specimen used was a bar, identified as 53B, which was produced by du Pont during their early commercialization of the material. The bar was annealed at 1100^o C for 1 hour in vacuum prior to examination. This material had an average particle size of about 0.03 micron, whereas currently produced TD-Nickel is said to have a finer particle size, of less than 0.02 micron (unpublished data from W. Pollock of du Pont).

Other nickel alloys examined were three compacted blends of nickel and alumina powders. One of the blends also had an admixture of nickel oxide. Two of the compacted blends were selected out of a large number which were examined in the SEEM as part of a study of blending techniques. For both blends, alumina of particle size 0.02 micron was used, but the nickel powder particle sizes were different, being 1 to 2 microns for one and 0.02 micron for the other. These two specimens were chosen to demonstrate the use of the SEEM as a screening test for evaluating blends of metal and oxide powders.

A blend of nickel, nickel oxide, and alumina was made for exposure to a number of combinations of ion species, discharge voltages, and specimen temperatures in the SEEM to determine whether fine alumina could be distinguished from fine nickel oxide.

The aluminum alloy M-257, containing a nominal 5 weight percent of alumina, was included as representative of the sintered aluminum powder type.

The three tungsten-base alloys came from current work at Lewis. Tungsten with coarse thoria particles was chosen to illustrate the sharp, high-contrast pictures obtainable in the SEEM when particles are well above the resolution limit. Tungsten with fine thoria and a tungsten-tantalum alloy were examined in the SEEM because earlier examination by etching, replication, and the use of the CEM had not given micrographs in which

TABLE II. - MATERIALS EXAMINED

Item	Nominal composition		Condition	Source	Located in figure -
	Matrix	Dispersoid			
1	Nickel	2 vol. % fine ThO_2	As-annealed bar	DuPont TD-Ni	4 and 5
2	Inco B nickel (1 to 2μ)	1.4 vol. % Al_2O_3 (Alon C)	Dry blended, explosively compacted	Nickel, International Nickel; Alumina, Godfrey L. Cabot Co.	16
3	Nickel (submicron)	8 vol. % Al_2O_3	Wet blended, explosively compacted	Powders from Vitro Corp., blended at NASA Lewis	17
4	Nickel	2.5 vol. % NiO , 2.5 vol. % Al_2O_3	Dry-blended, explosively compacted	Nickel, Union Carbide Metals; oxides, Vitro Corp.	13
5	Aluminum	5 wt. % Al_2O_3	As-received bar	Alcoa M-257	18
6	Tungsten	5 vol. % coarse ThO_2	As extruded	NASA Lewis	9 and 10
7	Tungsten	5 vol. % fine ThO_2	As extruded		7
8	Tungsten plus 5 wt. % Ta	0.1 vol. % ZrO_2	As extruded		19
9	Foil laminate containing W, Hf, Zr, Ta, Al, Ni, Ti	-----	As pressed		14
10	Unidirectionally solidified Al-CuAl ₂ eutectic (lamellar)	-----	As-received bar	United Aircraft Research Lab.	15
11	Unidirectionally solidified Al-NiAl ₃ eutectic (rod-like)	-----	As-received bar	United Aircraft Research Lab.	3

phases were clearly distinguished.

A composite metal foil laminate of titanium, zirconium, tantalum, hafnium, tungsten, nickel, and aluminum was prepared to show their relative "brightness" in the SEEM (for one operating condition).

The unidirectionally solidified eutectics, Al-CuAl₂ and Al-Al₃Ni were included to illustrate the appearance of two-phase all-metal microstructures and to allow measurements to be made on them for calculation of resolution limit.

Specimen Preparation for SEEM Examination

Preparation for fully dense materials, such as extruded bar stock and unidirectionally solidified eutectics, involved mounting in a specimen holder followed by polishing according to the following procedure. Materials received as powders were explosively compacted in a cartridge-actuated compaction press (ref. 7) and then mounted and polished. Only specimens whose density was in excess of 85 percent of theoretical were examined in this study. The foil laminate was prepared by encapsulating various metal foils in aluminum foil. After the capsule was imbedded in a conducting mounting powder and pressed in a metallographic mounting press, it was sectioned, cut to fit a specimen holder, and then polished.

After the specimens were mounted in SEEM specimen holders, all samples were polished according to the following sequence: papers through number 600, white silk satin with 3-micron diamond compound, and gamal cloth with 1/4-micron diamond compound. Polishing debris was removed by repeated alcohol washings. With compacts of relatively low density, ultrasonic cleaning of the polished specimens was found to be desirable.

Replication for Conventional Electron Microscopy

Replication was used in obtaining conventional electron micrographs. The preceding polishing procedure for specimens was followed and after etching with an appropriate etchant, two-stage carbon-Mowital replicas were prepared. Replicas were shadowed with urania. A Philips Electron Microscope (Model EM100B) was used.

Particle Sizing and Counting

A Zeiss Particle Size Analyzer (model TGZ-3), which can be used to record data on either a distributive or cumulative basis, was used to count and size dispersoid particles on electron micrographs (ref. 8). The "particles" so counted represent intercepts of

the plane of polish with the three-dimensional dispersoid particles in the original specimen. Throughout this paper, the two-dimensional intercepts observed in the micrographs will be referred to simply as particles.

The size distributions of particles were measured in micrographs of TD-Nickel and a tungsten-thoria dispersion alloy both as observed in the SEEM and in a conventional electron microscope. To insure that sufficient particles were counted to reduce effects of local inhomogeneities in the oxide distribution, several micrographs of each specimen were generally used. For example, 3 SEEM micrographs and 10 CEM micrographs of TD-Nickel were measured. These data were used to measure the preferential enlargement of oxide particle images occurring in the SEEM.

Determination of SEEM Resolution Limit

In this study the resolution limit is defined as the minimum separation between two microstructural features clearly distinguishable as such in a photomicrograph. To avoid the distortion found in oxide images (which will be discussed in the following section), an all-metal system was examined. A rodlike unidirectionally solidified eutectic, supplied by United Aircraft Research Laboratories, was chosen on the basis of its unusually uniform microstructure. Although the "rods" and their spacing proved to be too large to use directly, the separation of fine topographic features in the etched microstructure could be used to determine the resolution limit.

Experiments for Explanation of "Volume Percent Anomaly"

To determine the nature of the volume percent anomaly, a comparison was made between the particle densities (number of particles per unit area) and sizes measured by secondary emission microscopy and by conventional electron microscopy (replication). When it was determined that there was a selective enlargement of oxide particle images, particle sizing and counting measurements were made to explore the variability of this enlargement and to establish enlargement factors for selected materials.

Additional experiments were run to determine whether penetration of the ion beam into the specimen and the ion beam etching rate contributed to the volume percent anomaly.

Investigation of Phase Discrimination

In this study phase discrimination is defined as the ability to distinguish between two distinct phases in a microstructure. Three classifications of phase discrimination were investigated: metal/oxide, oxide/oxide, and metal/metal. Dispersions of alumina, thoria, and nickel oxide in nickel; thoria and zirconia in tungsten; and alumina in alumi-

TABLE III. - PHASE DISCRIMINATION
EXPERIMENTS

Series	Bombarding ion	Discharge potential, kV	Specimen temperature, °C
A	Hydrogen, argon nitrogen, air	35	445
B	Nitrogen	34, 30, 26, 22, 18	430
C	Nitrogen	30	40, 155, 250, 325, 390, 525

num were examined to show metal/oxide contrast.

Oxide/oxide discrimination was investigated by observing a prepared blend of nickel, nickel oxide, and alumina. A specific region in this material was examined with various bombarding ions at constant specimen temperature and ion discharge potential. Similar experiments were made using specimen temperature and ion discharge potential as variables. The various experiments are summarized in table III.

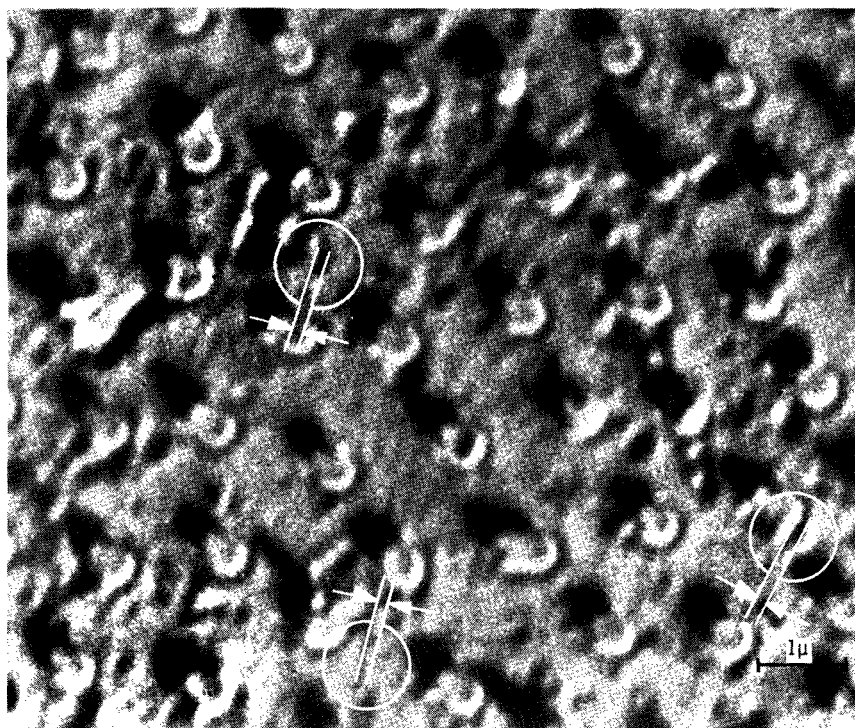
The possibility of discrimination between metals in the SEEM was investigated by examining a lamellar, unidirectionally solidified Al-CuAl₂ eutectic and also a section through the foil laminate.

RESULTS

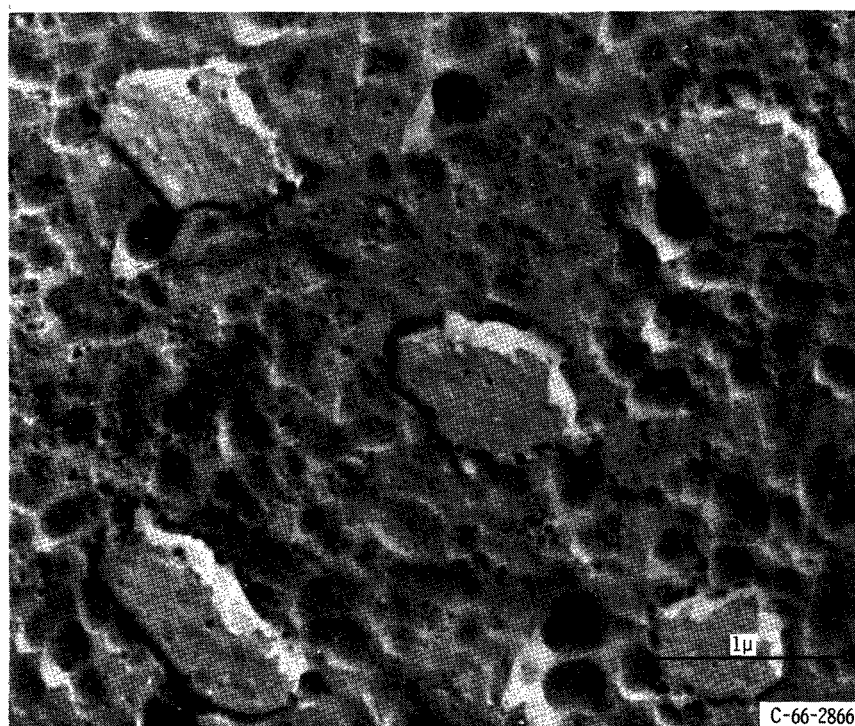
Secondary Electron Emission Microscope (SEEM) Resolution Limit

The electron micrographs shown in figure 3 were used in determining the working resolution limit of the SEEM. Each shows the microstructure of a transverse section of a rodlike unidirectionally solidified Al-Al₃Ni eutectic. Figure 3(a) was obtained with the SEEM. The microstructure was imaged at a magnification of 660 and photographically enlarged from this value to a magnification of 12 000 for measurement. The working resolution limit, that is, the resolution limit readily achievable under typical operating conditions, was established by measuring the minimum detectable separation between surface features. Examples of features measured are indicated by the arrows in figure 3(a). From these measurements a working resolution limit of about 800 Å (0.08 μ) was determined.

Figure 3(b) shows a conventional electron micrograph of the same microstructure obtained by replication. A much higher print magnification (×27 000) is permitted because of the superior resolving power of the conventional electron microscope. Surface details smaller than 800 Å (0.08 μ) are clearly distinguishable. Note that in figure 3(a) (p. 13) the peripheries of the rods of the eutectic structure appear to be smooth and rounded, while from figure 3(b) (CEM) it is evident that they are actually irregular.



(a) As examined with the SEEM. Viewed at room temperature with 15-kilovolt nitrogen ions. (Smallest resolvable features of 800Å, or 1 millimeter, are indicated.) X 12 000.



(b) As examined with a conventional electron microscope (CEM). X27 000.

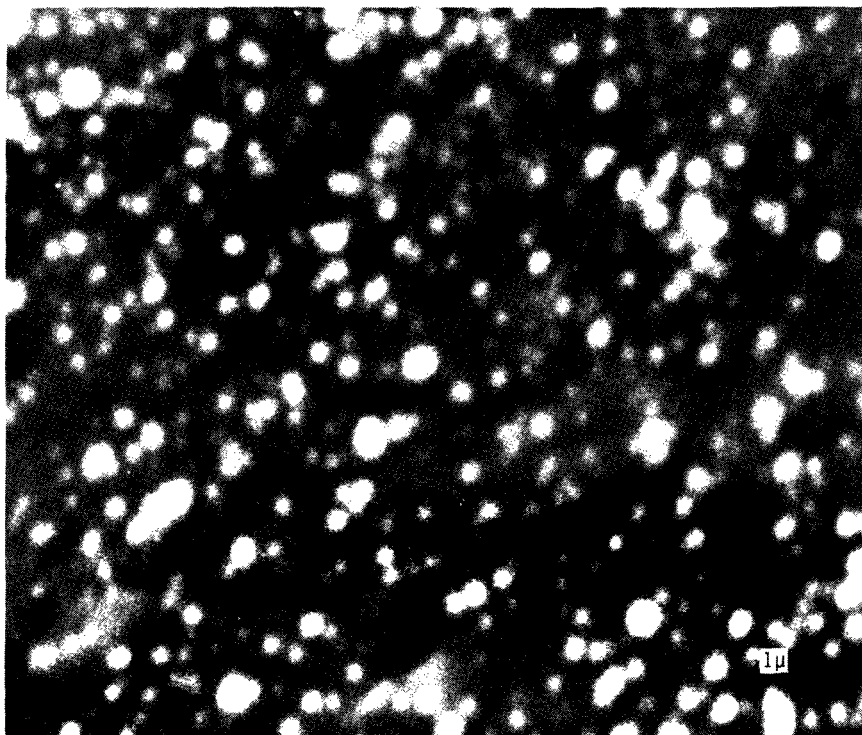
Figure 3. - Micrographs of unidirectionally solidified rodlike Al-Al₃Ni eutectic. Transverse solidification direction. Etchant, 10 parts glycerine - 15 parts hydrofluoric acid - 85 parts water.

TABLE IV. - PARTICLE SIZE DISTRIBUTION IN TD-NICKEL ALLOY FROM SEEM^a

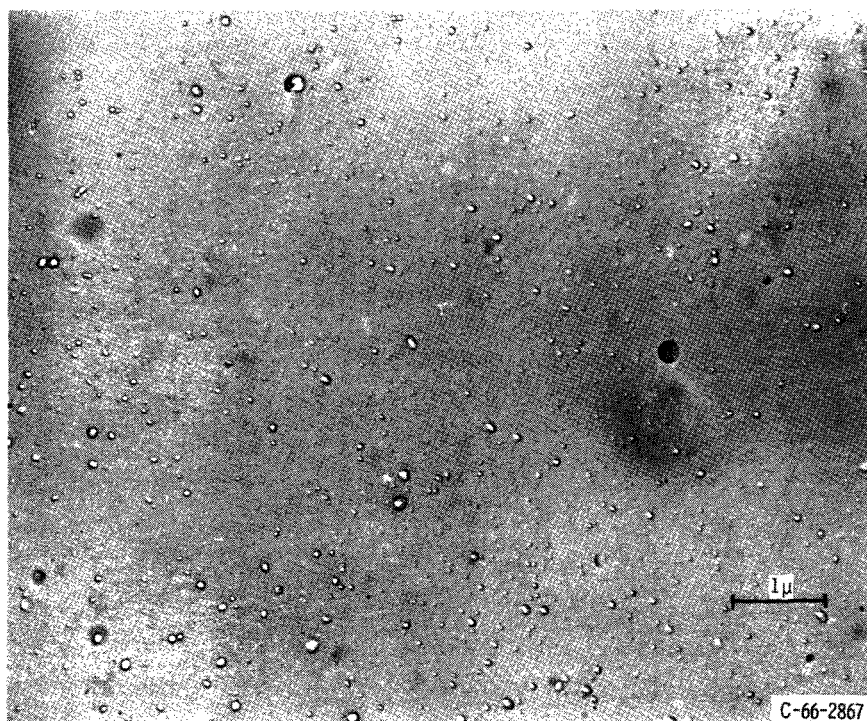
[Counted on Zeiss Instrument in mode: exponential response, distributive data, reduced range.]

Zeiss counter	Upper limit of size range, μ	Number of particles counted		Cumulative percent of particles finer than stated size
		Distributive	Cumulative	
5	0.049	1	1	0.02
6	.053	3	4	.09
7	.056	6	10	.22
8	.060	12	22	.48
9	.064	37	59	1.29
10	.069	59	118	2.58
11	.073	74	192	4.19
12	.078	146	338	7.38
13	.083	181	519	11.3
14	.089	200	719	15.7
15	.094	235	954	20.8
16	.101	240	1194	26.1
17	.108	234	1428	31.2
18	.116	276	1704	37.2
19	.123	287	1991	43.5
20	.131	301	2292	50.1
21	.140	301	2593	56.6
22	.150	268	2861	62.5
23	.160	224	3085	67.4
24	.170	212	3297	72.0
25	.182	211	3508	76.6
26	.194	183	3691	80.6
27	.207	170	3861	84.3
28	.221	201	4062	88.7
29	.236	125	4187	91.4
30	.252	93	4280	93.5
31	.269	74	4354	95.1
32	.287	52	4406	96.2
33	.306	47	4453	97.2
34	.327	32	4485	97.9
35	.349	33	4518	98.7
36	.372	17	4535	99.0
37	.398	12	4547	99.3
38	.424	11	4558	99.5
39	.453	7	4565	99.7
40	.483	5	4570	99.8
41	.516	4	4574	99.9
42	.551	2	4576	↓
43	.588	1	4577	
44	.628	1	4578	
45	.670	0	4578	
46	.715	0	4578	↓
47	.763	1	4579	
				100.0

^aSee fig. 4(a) for micrograph of specimen. $\times 12\ 000$.



(a) As examined with SEEM. Viewed at 460° C with 17.5-kilovolt nitrogen ions.



(b) As examined with CEM. Etchant, nickel.

Figure 4. - Micrographs of extruded, annealed TD-Nickel alloy (nickel - 2 vol. % thoria). Transverse section. X12 000.

TABLE V. - PARTICLE SIZE DISTRIBUTION IN TD-NICKEL ALLOY FROM CEM^a

[Counted on Zeiss counter in mode: exponential response, distributive data, reduced range.]

(a) Complete distribution.

Zeiss counter	Upper limit of size range, μ	Number of particles counted		Cumulative percent of particles finer than stated size
		Distributive	Cumulative	
1	0.0096	3	3	0.10
2	.0102	5	8	.27
3	.0109	9	17	.57
4	.0116	9	26	.88
5	.0124	17	43	1.45
6	.0133	14	57	1.92
7	.0142	41	96	3.24
8	.0151	47	143	4.83
9	.0162	82	225	7.60
10	.0173	103	328	11.1
11	.0184	147	475	16.0
12	.0196	131	616	20.8
13	.0209	170	786	26.5
14	.0224	191	977	33.0
15	.0238	164	1141	38.5
16	.0256	166	1307	44.1
17	.0271	146	1453	49.1
18	.0291	157	1610	54.4
19	.0309	144	1754	59.2
20	.0331	133	1887	63.7
21	.0353	140	2027	68.4
22	.0378	101	2128	71.8
23	.0402	112	2240	75.6
24	.0429	113	2353	79.4
25	.0458	89	2442	82.4
26	.0489	59	2501	84.4
27	.0522	53	2554	86.2
28	.0558	67	2621	88.5
29	.0596	67	2688	90.7
30	.0637	53	2741	92.5
31	.0678	53	2794	94.3
32	.0722	40	2834	95.7
33	.0771	40	2874	97.0
34	.0824	22	2896	97.8
35	.0880	17	2913	98.3
36	.0938	12	2925	98.8
37	.100	9	2934	99.1
38	.107	10	2944	99.4
39	.114	7	2951	99.6
40	.122	4	2955	99.8
41	.130	4	2959	99.9
42	.139	1	2960	↓ 100.0
43	.148	0	2960	
44	.158	0	2960	
45	.169	1	2961	
46	.180	0	2961	↓ 100.0
47	.192	1	2962	

^aSee fig. 5 for micrograph of specimen. $\times 45\ 000$.

TABLE V. - CONCLUDED. PARTICLE SIZE DISTRIBUTION IN TD NICKEL ALLOY FROM CEM^a

[Counted on Zeiss counter in mode: exponential response, distributive data, reduced range.]

(b) Partial distribution for comparison with SEEM.

Zeiss counter	Upper limit of size range, μ	Number of particles counted, cumulative	Number of particles corresponding to top 32.8 percent of total (b)	Cumulative percent of particles finer than stated size, top 32.8 percent of particles only (b)
1	0.0096	3	---	---
2	.0102	8	---	---
3	.0109	17	---	---
4	.0116	26	---	---
5	.0124	43	---	---
6	.0133	57	---	---
7	.0142	96	---	---
8	.0151	143	---	---
9	.0162	225	---	---
10	.0173	328	---	---
11	.0184	475	---	---
12	.0196	616	---	---
13	.0209	786	---	---
14	.0224	977	---	---
15	.0238	1141	---	---
16	.0256	1307	---	---
17	.0271	1453	---	---
18	.0291	1610	---	---
19	.0309	1754	---	---
20	.0331	1887	---	---
21	.0353	2027	37	3.8
22	.0378	2128	138	14.2
23	.0402	2240	250	25.7
24	.0429	2353	363	37.3
25	.0458	2442	452	46.5
26	.0489	2501	511	52.6
27	.0522	2554	564	58.0
28	.0558	2621	631	64.9
29	.0596	2688	698	71.8
30	.0637	2741	751	77.3
31	.0678	2794	804	82.7
32	.0722	2834	844	86.8
33	.0771	2874	884	90.9
34	.0824	2896	906	93.2
35	.0880	2913	923	95.0
36	.0938	2925	935	96.2
37	.100	2934	944	97.1
38	.107	2944	954	98.1
39	.114	2951	961	98.9
40	.122	2955	965	99.3
41	.130	2959	969	99.7
42	.139	2960	970	99.8
43	.148	2960	970	99.8
44	.158	2960	970	99.8
45	.169	2961	971	99.9
46	.180	2961	971	99.9
47	.192	2962	972	100.0

^b Fourth and fifth columns correspond to size range visible in SEEM (32.8 percent of total particles).

Particle Size and Particle Image Enlargement

The results of measurements of thoria particle size distribution for TD-Nickel are tabulated in tables IV and V(a) (pp. 14 and 16). The micrographs in figures 4 (p. 15) and 5 are representative of those used for these measurements. Figure 4(a) shows a micrograph obtained with the SEEM, and figure 4(b) is the same microstructure examined with a CEM at the identical magnification of 12 000. The smallest particles visible in figure 4(b) were too small for convenient measurement so that micrographs, such as those in figure 5 at a magnification of 45 000, were used for counting and sizing particles, as shown by the CEM.

In tables IV and V(a) the particle size counts from SEEM and CEM micrographs are tabulated on both a distributive and cumulative basis. The former is necessary for calculation of the volume percent of the dispersed phase while the latter is convenient for comparing the results from the two sets of measurements. The largest particles observed in the SEEM appear to be much larger than the largest particles seen by the CEM. In addition, the median particle size (the 50 percent size from the cumulative data) for thoria from the SEEM micrographs is approximately five times that measured from the CEM. These data will be used to establish that the volume percent anomaly is caused by a preferential enlargement of individual oxide particle images beyond the general field magnifi-

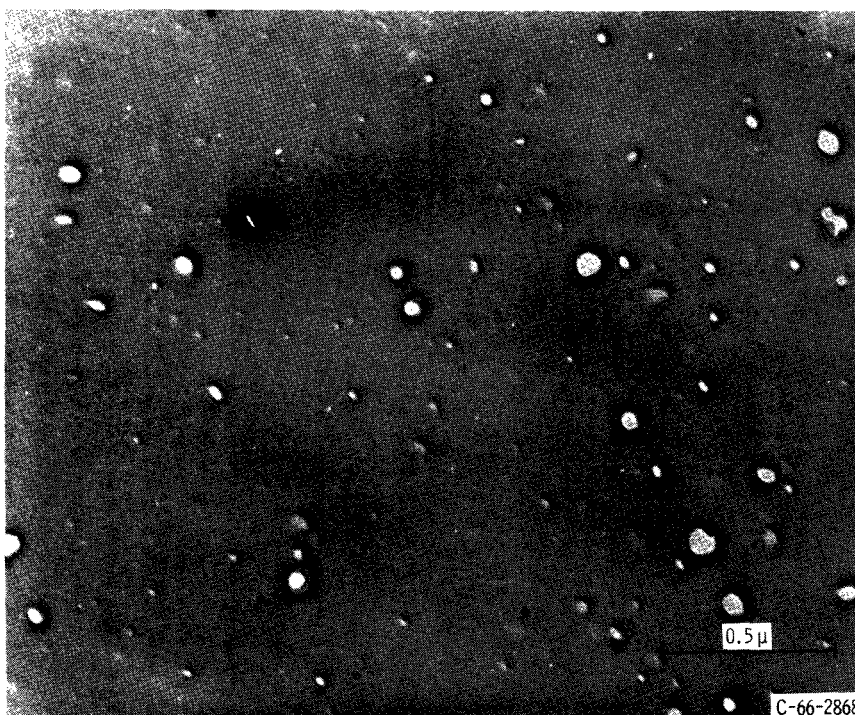


Figure 5. - CEM micrograph of extruded and annealed TD-Nickel alloy. Transverse section. Etchant, nickel. X45 000.

cation and to determine quantitatively the magnitude of this particle image enlargement.

In table VI are summarized the results of the particle counting and sizing measurements from a number of micrographs (e. g., figs. 4(a) and 5) from both types of microscopes. From these data the volume percents of thoria and the thoria particle densities (particles per unit area of specimen) obtained by the two methods can be compared.

The data show that, although the volume percent measured with the SEEM is 9.51, roughly six times the 1.62 percent shown in the CEM micrograph, the particle density in the SEEM micrographs is only about one-third that in the CEM micrographs. The lower particle density from the SEEM can give a higher volume percent only if each particle is individually enlarged. This finding that an enlargement of images from oxide particles gives rise to the volume percent anomaly raised another question: Is the enlargement factor for all particle images independent of particle size?

From the particle density results given in table VI, it can reasonably be assumed that the total particle population visible in the SEEM corresponds to only the top 32.8 percent of the particle population observed by the CEM ($4.74/14.4 \times 100$ percent). By comparing the corresponding sets, which represent only the particles visible in both instruments, the dependence of enlargement factor upon particle size can be determined.

Table V(a) was modified to consider only those particles visible in both the SEEM and the CEM. The result is table V(b) (p. 17) where the partial distribution representing the top 32.8 percent of the particle population observed in the CEM appears in the columns on the right.

Note that the cutoff point in table V(b) corresponds to a particle size of 0.035 micron. This may be taken as an approximate value for the detection limit for dispersoid particles observed in the SEEM, at least for thoria in a nickel matrix. Note also that this value is not very sensitive to errors in particle counting. Errors of ± 10 percent in either the SEEM or CEM particle counts would still leave a cutoff point and indicated detection limit between 0.03 and 0.04 micron.

The cumulative particle distributions from tables IV and V(b) are both plotted in

TABLE VI. - PARTICLE DENSITY IN TD-NICKEL ALLOY AS VIEWED IN SEEM AND CEM

Instrument	Area counted		Number of particles counted	Particle density, ^a particle/ μ^2	Volume percent ^b
	Micrograph, mm^2	Specimen field, μ^2			
SEEM	124 300	966	4579	4.74	9.51
CEM	415 300	205	2962	14.4	1.62

^aNumber of particles detected in SEEM is only $4.74/14.4 \times 100 = 32.8$ percent of number visible in CEM.

^b $(\sum \text{particle area} / \text{total area}) \times 100$ percent, from distributive data.

figure 6. If the enlargement factor were constant across the particle size range present, the SEEM curve would be displaced by a constant ratio from the CEM curve. By taking ratios at several points of cumulative percent in figure 6, the values in table VII were derived. The enlargement factor in the SEEM varied from about 2.3 to 3.3. Thus, for this size range of thoria particles in a nickel matrix, enlargement factors increased with increasing particle size.

A similar quantitative comparison of SEEM and CEM micrographs was made for the tungsten plus thoria microstructure shown in figure 7. (Measurements for the CEM case

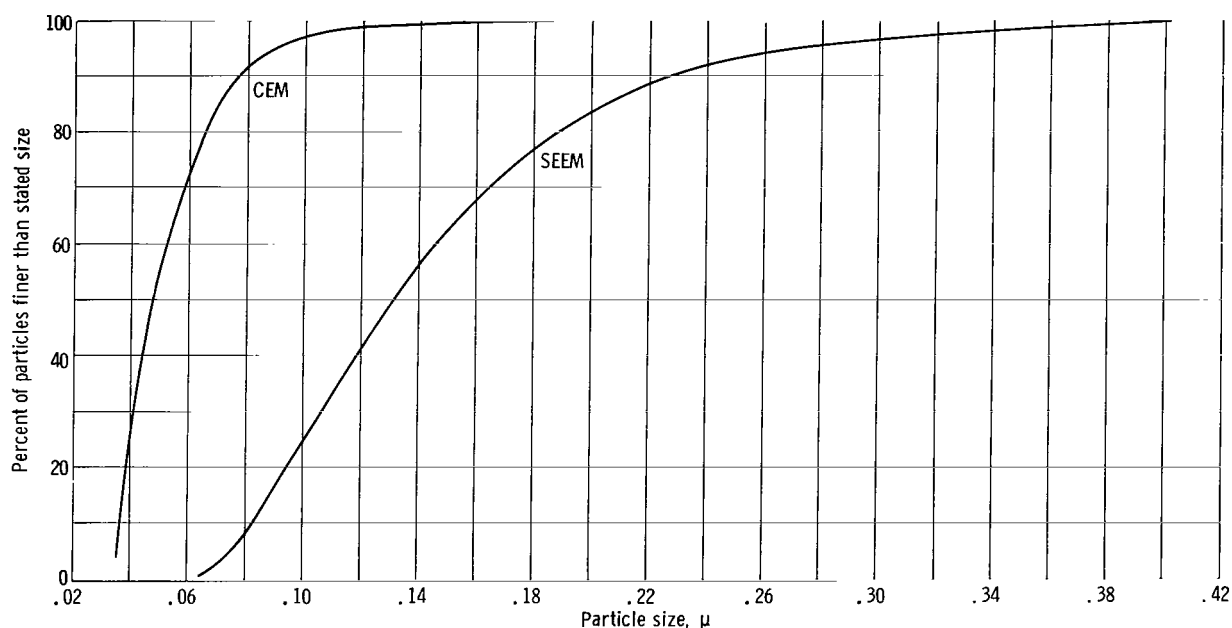
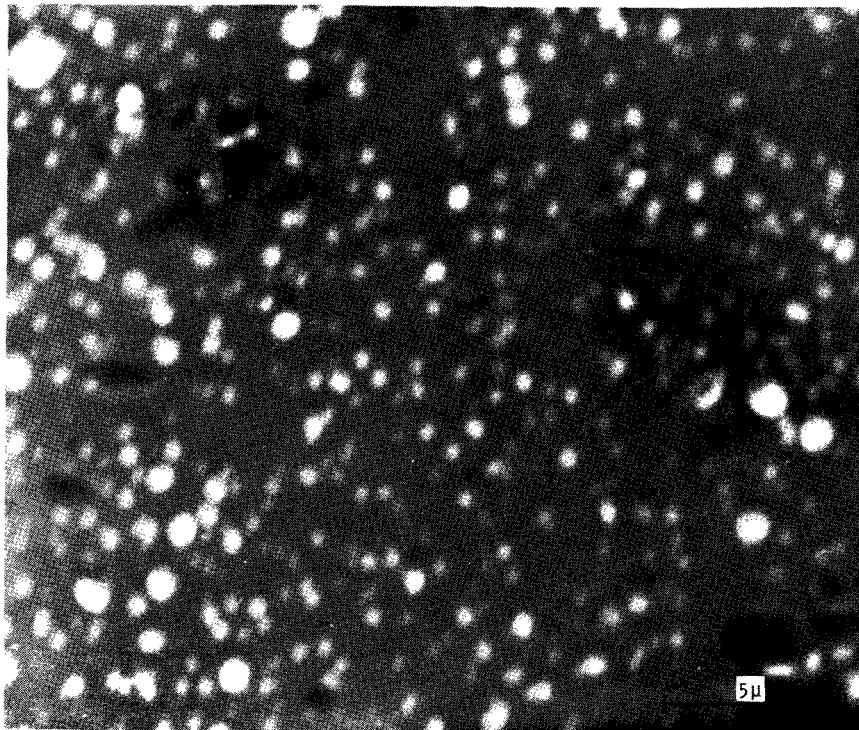


Figure 6. - Cumulative distributions of thoria particle sizes in TD-Nickel alloy by CEM and by SEEM considering only particles detected by both.

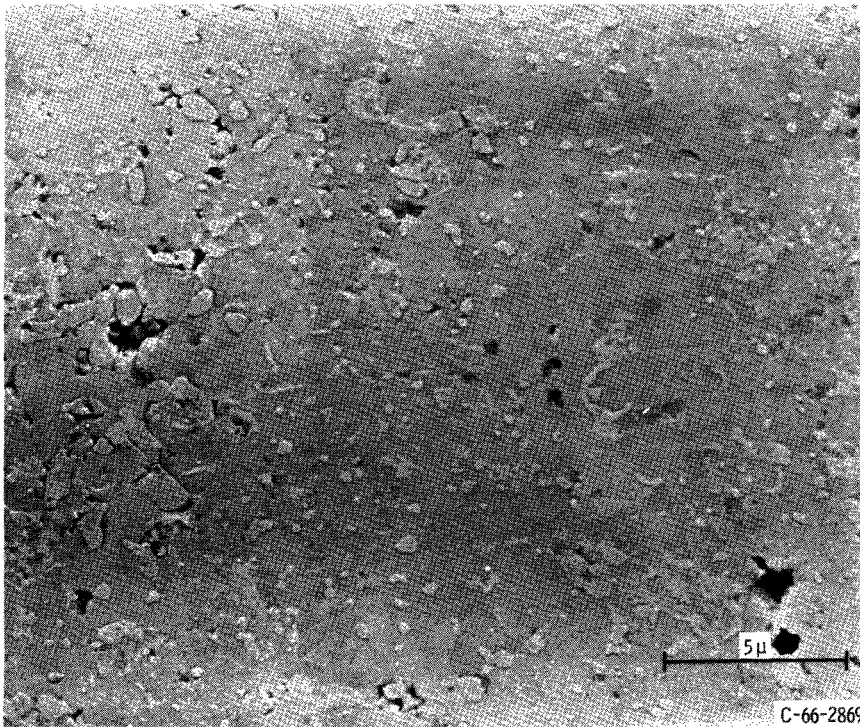
TABLE VII. - VARIATION OF PARTICLE ENLARGEMENT FACTOR IN SEEM

WITH PARTICLE SIZE FOR FINE THORIA IN TD-NICKEL ALLOY

Cumulative percent of particles finer than stated size	CEM particle size, μ	Apparent SEEM particle size, μ	Enlargement factor
15	0.038	0.088	2.3
30	.044	.107	2.4
50	.048	.131	2.7
75	.062	.178	2.9
95	.088	.269	3.1
99	.114	.372	3.3



(a) As examined with the SEEM. Viewed at 440° C with 15-kilovolt nitrogen ions. (Darkest regions are voids.)



(b) As examined with CEM. Etchant, 30 parts lactic acid - 10 parts nitric acid - 5 parts hydrofluoric acid.

Figure 7. - Micrographs of fine thoria particles in extruded tungsten - 5 volume percent thoria. Transverse section. X4800.

were made at $\times 10\,000$, a higher magnification than that given in figure 7(b).) As is shown in table VIII, the particle density, as viewed in both instruments, was approximately the same which indicated that all the particles present in this material were above the detection limit of the SEEM. The particle size distributions measured from the micrographs of figure 7 are tabulated in tables IX and X (pp. 23, 24, and 25). Particle size distributions from both instruments are plotted in figure 8 (p. 26). Table XI (p. 26), which was constructed from figure 8, shows that the enlargement factor for particle images in this tungsten plus thoria material is 2.3 at a true (CEM) particle size of 0.083 micron but drops to unity at a particle size of about 0.6 micron. This is contrary to the trend in TD-Nickel, where the enlargement factors increased with increasing particle size.

Particle enlargement was also measured in another specimen of tungsten-thoria material with coarser thoria particles. The general microstructure of this material is shown in figure 9 (p. 27). By means of a scratch on the specimen and an odd "boomerang-shaped" marker particle, it was possible to locate the identical grouping of particles in both SEEM and CEM micrographs (figs 10(a) and (b) (p. 28), respectively). The diameter of the nearly circular particle image next to the boomerang marker was 4.3 microns when measured by the SEEM and 3.3 microns when measured by a CEM. The enlargement factor here was 1.3.

Particle enlargement was also observed but not measured for alumina particles in nickel. In figure 11 (p. 29), which shows shadows cast by the alumina surface particles, the mismatch between image size and width of shadow is taken as evidence of image enlargement, as discussed in the appendix.

TABLE VIII. - PARTICLE DENSITY IN TUNGSTEN PLUS 5 VOLUME
PERCENT THORIA AS VIEWED IN SEEM AND CEM^a

Instrument	Area counted		Number of particles counted	Particle density, particle/ μ^2
	Micrograph, mm^2	Specimen field, μ^2		
SEEM	42 600 (at $\times 4800$)	1850	1535	0.83
CEM	127 900 (at $\times 10\,000$)	1280	1044	.82

^aSee fig. 7 for micrograph of specimen.

TABLE IX. - PARTICLE SIZE DISTRIBUTION IN TUNGSTEN PLUS 5 VOLUME PERCENT

THORIA FROM SEEM.^a

[Counted on Zeiss Instrument in mode: exponential response, cumulative data, reduced range.]

Zeiss counter	Upper limit of size range, μ	Number of particles counted, cumulative	Cumulative percent of particles finer than stated size
6	0.125	0	0
7	.133	3	0.20
8	.142	8	.52
9	.152	13	.85
10	.163	--	----
11	.173	55	3.6
12	.183	105	6.8
13	.196	163	7.6
14	.210	218	14.2
15	.223	282	18.4
16	.240	---	----
17	.254	431	28.1
18	.273	529	34.4
19	.290	648	42.2
20	.310	777	50.6
21	.331	901	58.7
22	.354	1020	66.4
23	.377	1107	72.1
24	.402	1187	77.3
25	.429	1267	82.5
26	.458	1324	86.3
27	.489	1375	89.6
28	.523	1401	91.3
29	.558	1429	93.1
30	.595	1447	94.3
31	.635	1472	95.9
32	.677	----	----
33	.723	1494	97.3
34	.772	1501	97.8
35	.825	1508	98.2
36	.879	1509	98.3
37	.939	1513	98.6
38	1.00	1520	99.0
39	1.07	1524	99.3
40	1.14	1528	99.5
41	1.22	1529	99.6
42	1.30	1529	99.6
43	1.39	1532	99.8
44	1.48	1533	99.9
45	1.58	1534	99.9
46	1.69	1535	100.0

^aSee fig. 7 for micrograph of specimen. $\times 4800$.

TABLE X. - PARTICLE SIZE DISTRIBUTION IN TUNGSTEN PLUS 5 VOLUME PERCENT THORIA FROM CEM.^a

[Counted on Zeiss Instrument in mode: exponential response, cumulative data, reduced range (except for counters marked with asterisk, where standard range was used).]

Zeiss counter	Upper limit of size range, μ	Number of particles counted, cumulative	Number of particles corresponding to 100 percent of particles (b)	Cumulative percent of particles finer than stated size for 100 percent of particles (b)
4	0.052	0	0	0
5	.056	1	1	0.10
6	.060	3	3	.29
7	.064	7	7	.67
8	.068	13	13	1.25
9	.073	19	19	1.82
10	.078	29	29	2.78
11	.083	47	47	4.50
12	.088	72	72	6.90
13	.094	96	96	9.20
14	.101	128	128	12.26
15	.107	165	165	15.80
16	.115	196	196	18.8
17	.122	236	236	22.6
18	.131	272	272	26.1
19	.139	308	308	29.5
20	.149	356	356	34.1
21	.159	399	399	38.2
22	.170	462	462	44.3
23	.181	513	513	49.1
24	.193	563	563	53.9
25	.206	616	616	59.0
26	.220	673	673	64.4
27	.235	723	723	69.3
28	.251	761	761	72.9

12 *	.265	762	762	73.0
29	.268	807	807	77.3
30	.286	830	830	79.5
31	.305	854	854	81.8
32	.325	884	884	84.7
33	.347	910	910	87.2
34	.371	923	923	88.4
35	.396	945	945	90.5
36	.422	951	951	91.1
37	.451	960	960	91.9
38	.481	971	971	93.0
39	.514	976	976	93.5
23 *	.543	977	977	93.6
40	.548	987	987	94.5
24 *	.580	988	988	94.6
41	.585	991	991	94.9
42	.625	997	997	95.4
43	.667	1000	1000	95.8
27 *	.705	1001	1001	95.9
44	.712	1010	1010	96.7
45	.760	1019	1019	97.6
46	.811	1022	1022	97.9
47	.865	1025	1025	98.2
31 *	.915	1027	1027	98.4
48	.924	1033	1033	98.9
32 *	.976	1034	1034	99.0
35 *	1.187	1035	1035	99.1
36 *	1.27	1036	1036	99.2
38 *	1.44	1038	1038	99.4
40 *	1.64	1041	1041	99.9
41 *	1.76	1043	1043	99.9+
42 *	1.87	1044	1044	100.0

^aFig. 7(b), but for micrograph at $\times 10\ 000$.

^bFourth and fifth columns correspond to size range visible in SEEM (100 percent).

TABLE XI. - VARIATION OF PARTICLE ENLARGEMENT FACTOR IN SEEM
WITH PARTICLE SIZE FOR FINE THORIA IN TUNGSTEN

Cumulative percent of particles finer than stated size	CEM particle size, μ	Apparent SEEM particle size, μ	Enlargement factor
5	0.083	0.190	2.3
15	.108	.215	2.0
30	.140	.258	1.8
50	.183	.310	1.7
75	.260	.390	1.5
95	.585	.612	1.0
99	.976	1.000	1.0
Single measurement of coarse thoria particle (fig. 10)	3.3	4.3	1.3

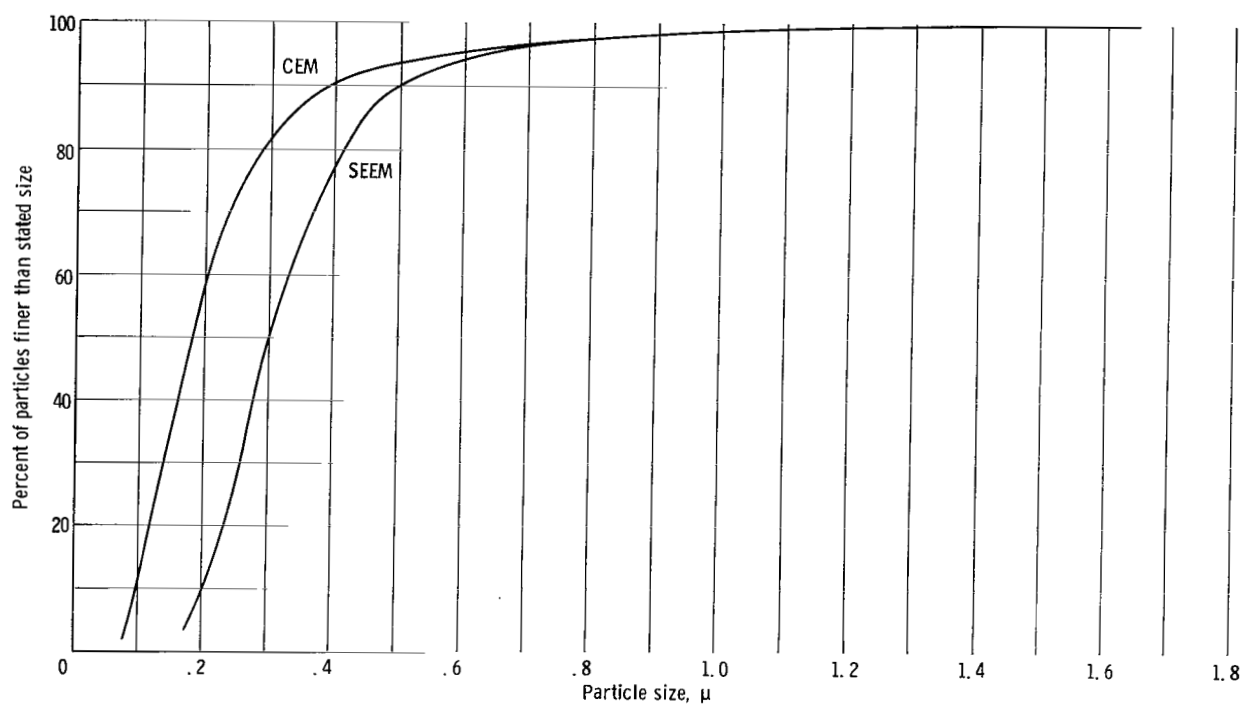
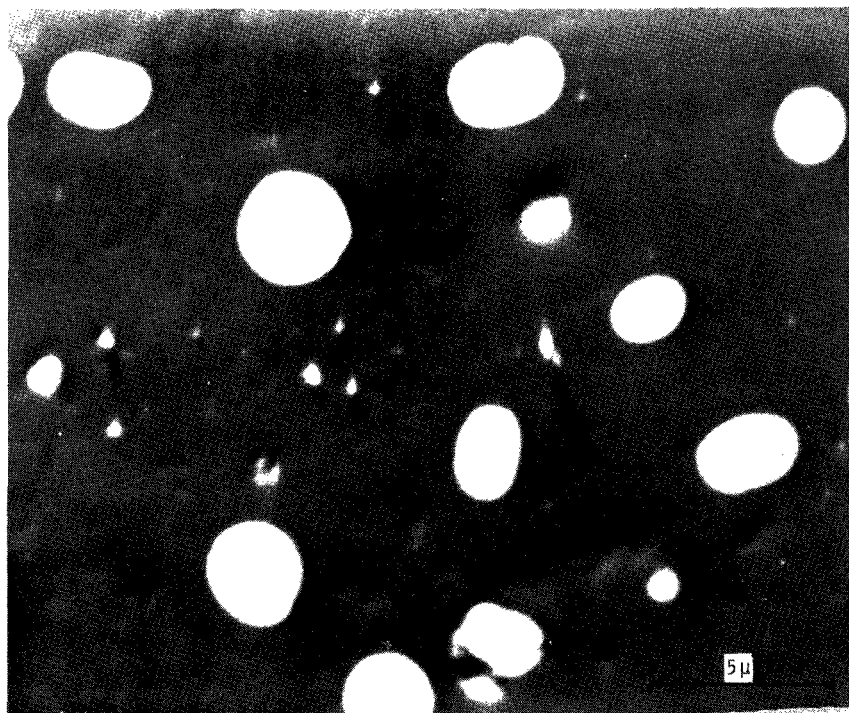
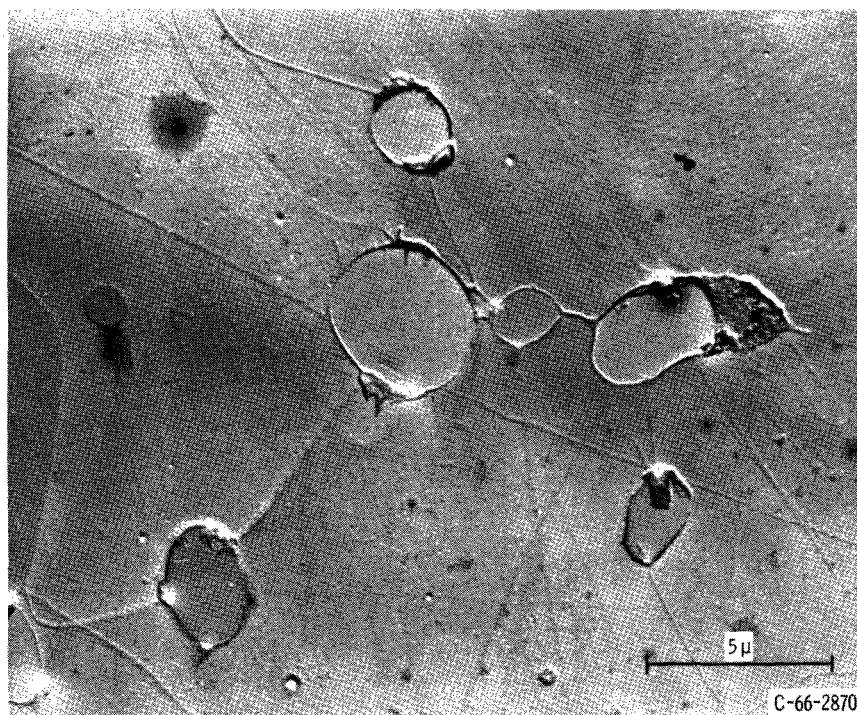


Figure 8. - Cumulative distributions of thoria particle sizes in TD-Nickel alloy by CEM and by SEEM.

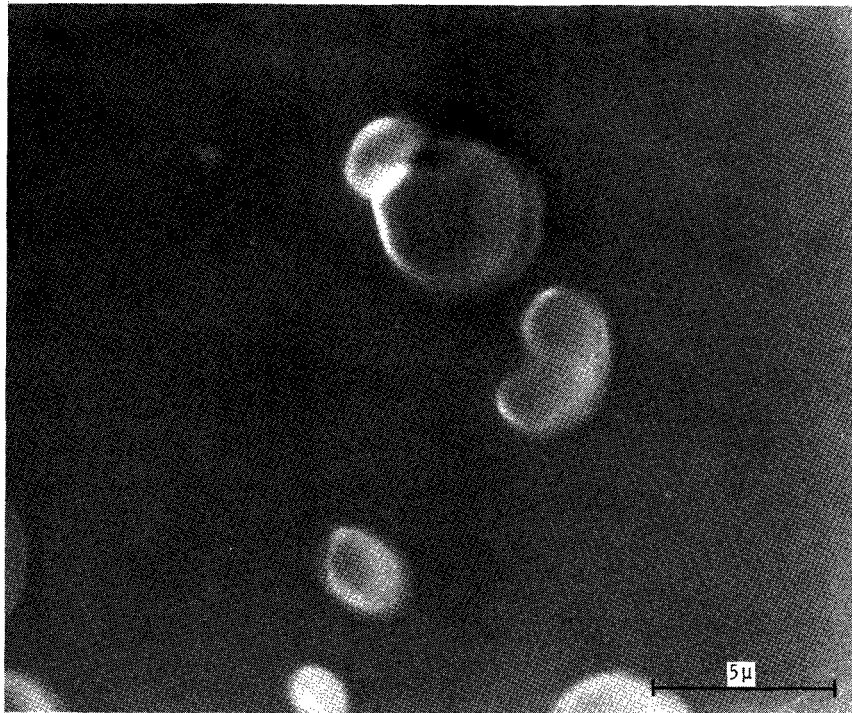


(a) As examined with SEEM. Viewed at 450° C with 17.5-kilovolt nitrogen ions.

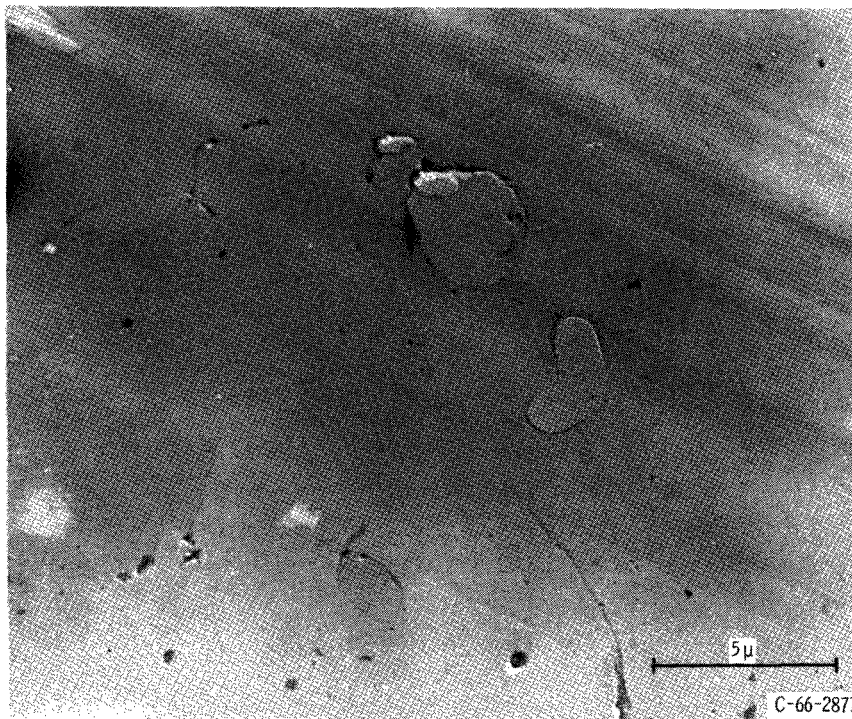


(b) As examined with CEM. Etchant, 30 parts lactic acid - 10 parts nitric acid - 5 parts hydrofluoric acid.

Figure 9. - Micrographs of coarse thoria particles in extruded tungsten - 5 volume percent thoria. Transverse section. X4800.

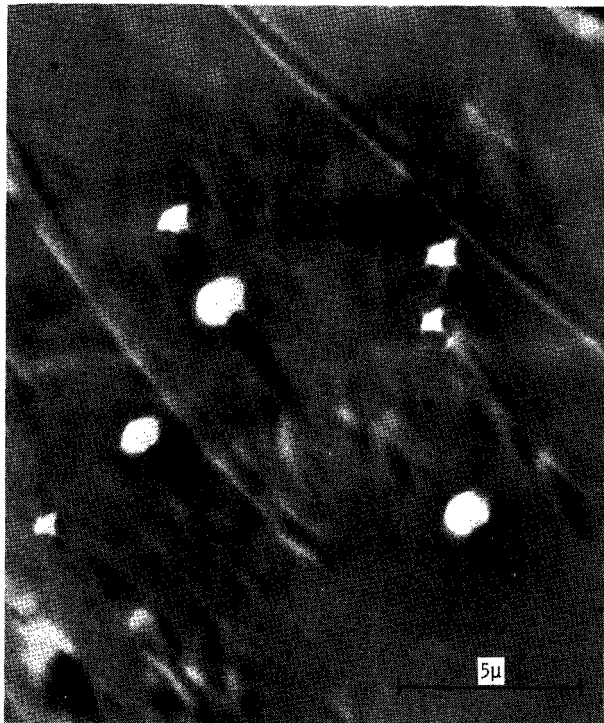


(a) As examined with SEEM. Viewed at 390° C with 15-kilovolt nitrogen ions.

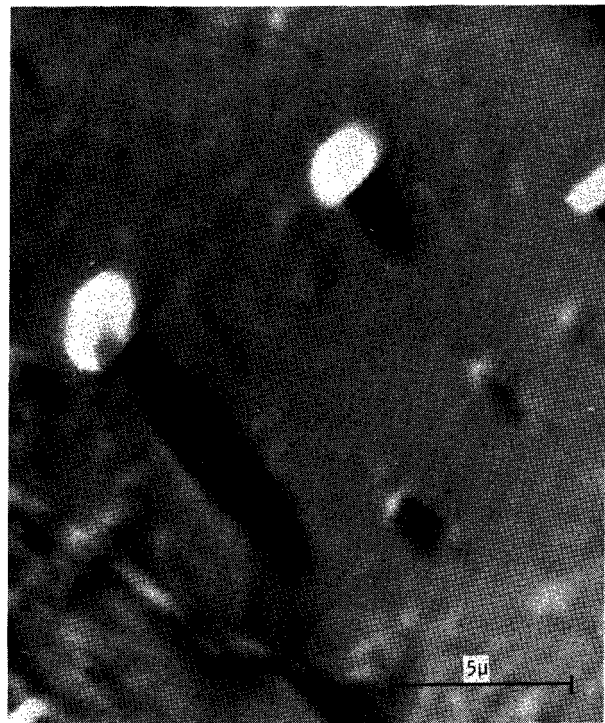


(b) As examined with CEM. Etchant, 30 parts lactic acid - 10 parts nitric acid - 5 parts hydrofluoric acid.

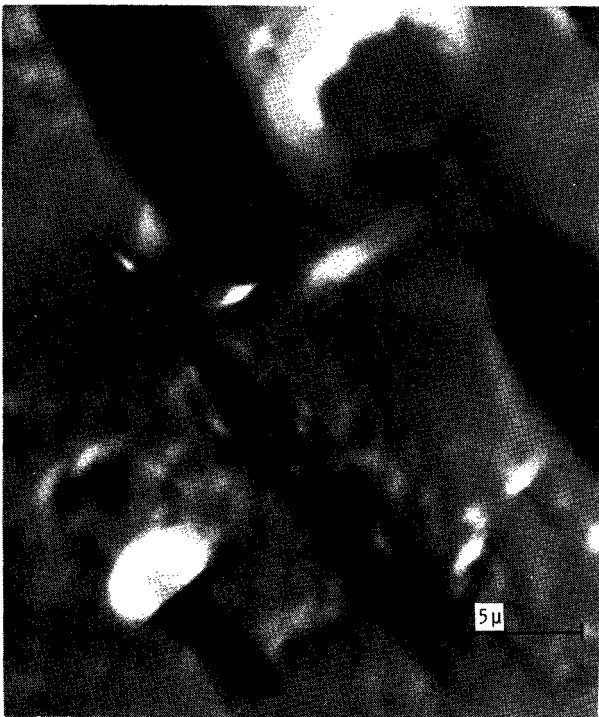
Figure 10. - Micrographs of coarse thoria particles in tungsten (see fig. 9) showing area examined with SEEM and CEM. X4700.



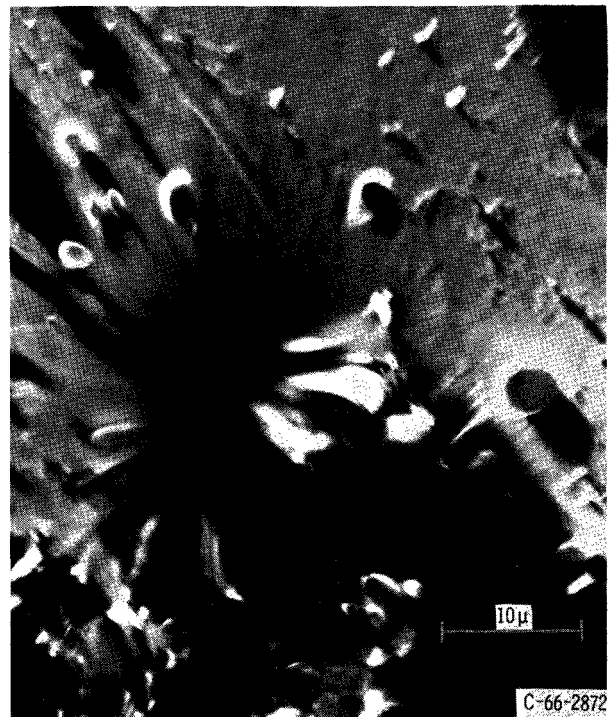
(a) Small alumina particles whose shadows lie only outside the apparent particle size. X4800.



(b) Larger alumina particles whose shadows lie partially within the apparent particle size. X4800.



(c) Larger alumina particles whose shadows lie partially within the apparent particle size. X4800.



(d) Persistent distortion of unknown origin. X1850.

Figure 11. - SEEM micrographs of alumina particles resting on film of colloidal silver. Viewed at 440° C with 17.5-kilovolt nitrogen ions.

Results of Experiments to Determine Ion Beam Penetration

Additional experiments to solve the volume percent anomaly indicated that the ion beam in the SEEM did not penetrate the surface of a metal specimen to an appreciable depth. The ion beam etching rate was also very low. These results were taken as evidence that oxide particles lying below the specimen surface are not imaged.

When a film of approximately 0.03 micron of nickel, as measured with a Zeiss interference microscope, was vacuum-evaporated onto the TD-Nickel specimen, the thoria dispersion was not visible in the SEEM; only the dark image characteristic of pure nickel was seen. On continuous observation with a low ion beam current, it was noted that the dispersion did not appear gradually in the image; rather the final number and size of thoria particles emerged suddenly when the ion beam had swept away much of the nickel layer.

The sudden appearance of the complete specimen structure implies that either the ion etching rate (surface removal) is high or that the ion penetration (subsurface illumination) is small. If penetration were substantial, a gradually increasing amount of oxide would be expected in the image because removal of the deposited layer allows an increasing depth of the specimen to be illuminated; however, the observed rapid appearance of the oxide image indicates that the ion beam penetration is small.

Another possibility considered was that a rapid ion etching rate, combined with the long photographic exposure times required, might result in micrographs containing images of particles originally below the surface as well as those originally at the surface. If the etching rate by the ion beam were large, the specimen surface would be rapidly swept away. Then, in the 6 to 8 seconds that the shutter to the plate cassette is open in photographically recording the electron image, oxide particles at various depths would become exposed. Since the specimen structure appeared in about 4 minutes under the experimental conditions (0.03 μ film of nickel on the surface, examination with 15-kV nitrogen ions at 25- μ A beam current), the etching rate of nickel must be on the order of 0.0001 to 0.0002 micron per second (0.03 μ /240 sec). The same rate was measured when gold rather than nickel was deposited. With an etching rate of 0.0002 micron per second, the surface of the specimen would be lowered 0.0014 micron during the 7-second exposure required for a typical photograph. This surface lowering represents less than 5 percent of the diameter of an average thoria particle in TD-Nickel (0.03 μ) and so could not account for the observed large increase in area fraction of dispersoid.

Results of Investigation into Irregular Ion Beam Etching

The extent to which irregular ion beam etching might contribute to the volume per-

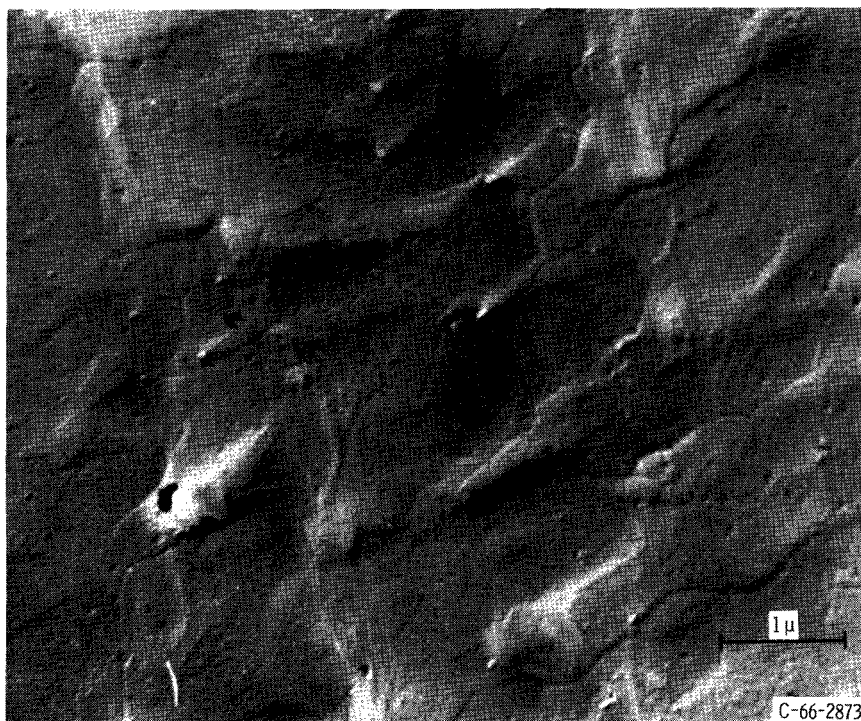
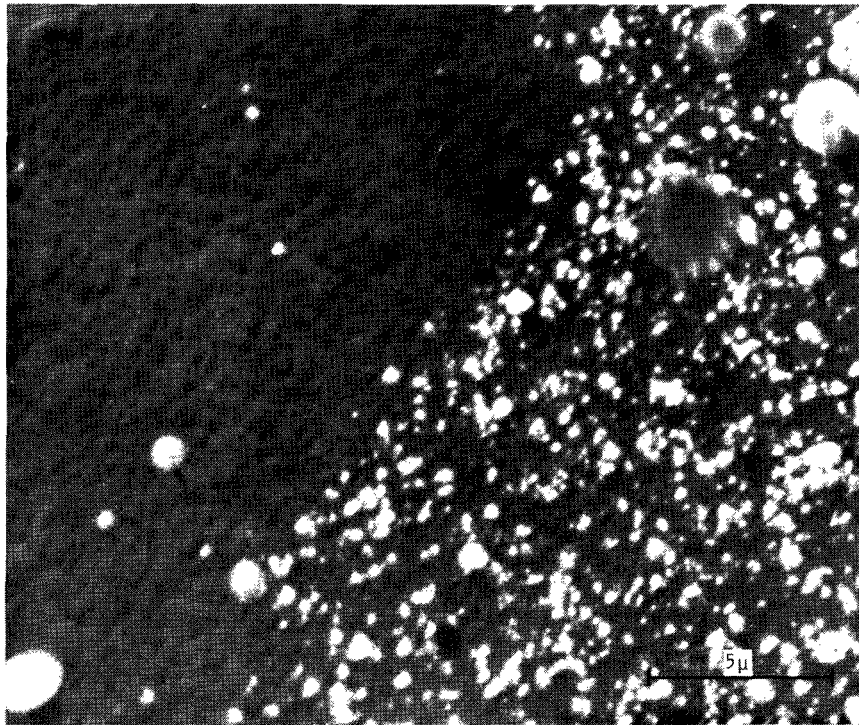


Figure 12. - CEM micrograph from replication of surface of TD-Nickel alloy after examination in SEEM (see fig. 4(a)). Unetched except by ion bombardment. X16 000.

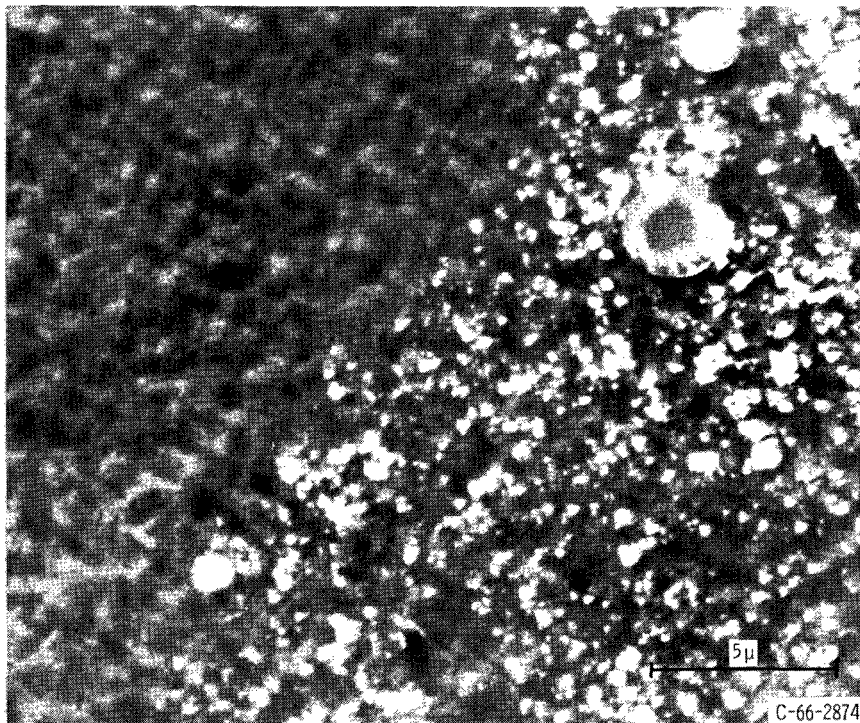
cent anomaly was experimentally determined. The results of examining the surface of a specimen in the CEM after exposure in the SEEM show that surface roughening caused by uneven ion etching is too small to give a hill-and-valley topography, which could expose large numbers of particles originally at various depths below the unetched surface. The extent of roughening usually present is shown in figure 12, which shows a conventional electron micrograph obtained by replication of a specimen directly after normal observation (with low ion beam current) in the SEEM (see fig. 4(a), p. 15). Since 45° shadowing was used in figure 12, the lengths of the shadows from steps on the surface are equal to the step height, or about 300 \AA . This step height is of the same order of magnitude as the average thoria particle size.

Phase Discrimination in Oxide/Oxide and Metal/Metal Systems

The results of attempts to measure the phase discrimination capabilities of the SEEM in oxide/oxide and metal/metal systems are summarized in figures 13 and 14, respectively. Figure 13 consists of selected micrographs from a series of experiments with a triple blend of nickel, nickel oxide, and alumina. A comparison of figures 13(a), (b), and (c) shows that the use of hydrogen, argon, and air as discharge ion species did not give a

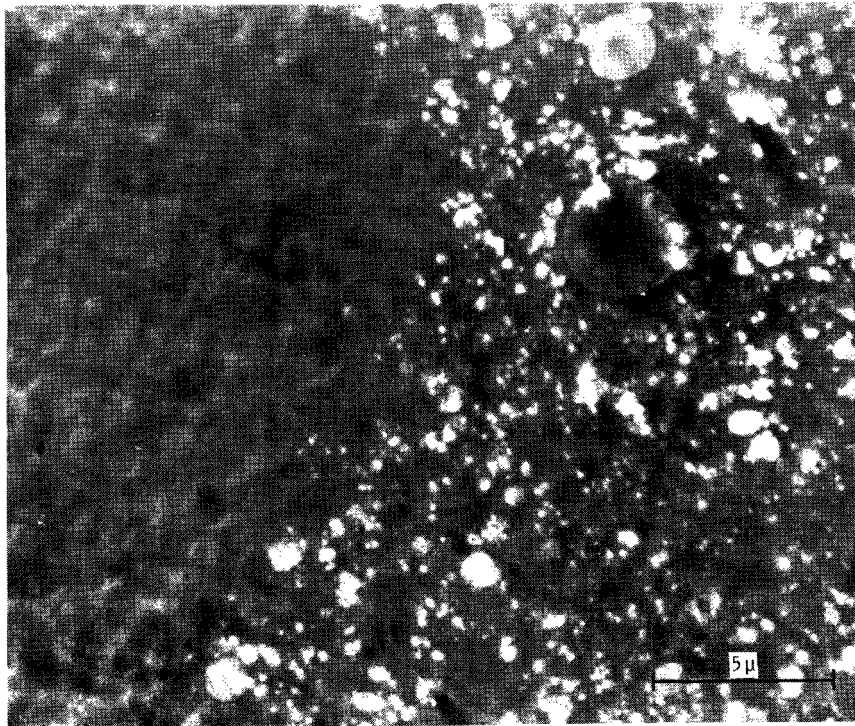


(a) Bombarding ion, hydrogen.

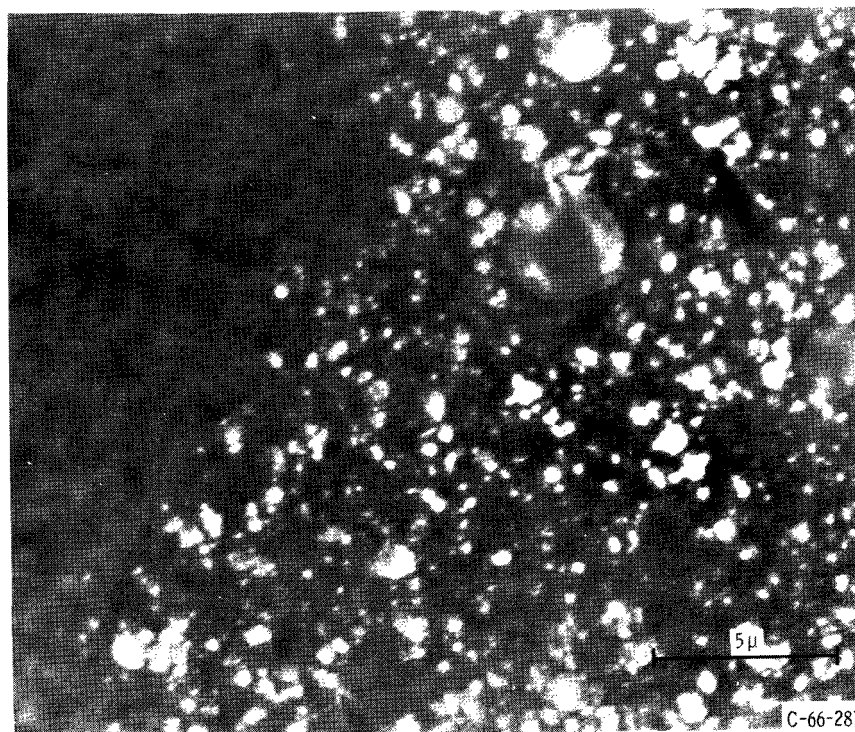


(b) Bombarding ion, argon.

Figure 13. - SEEM photomicrographs of triple blend of nickel - 2.5 volume percent nickel oxide - 2.5 volume percent alumina, dry-blended and explosively compacted. Examined at 445° C with various ions at 17.5 kilovolts. X4800.



(c) Bombarding ion, air.



(d) Bombarding ion, hydrogen.

Figure 13. - Concluded.

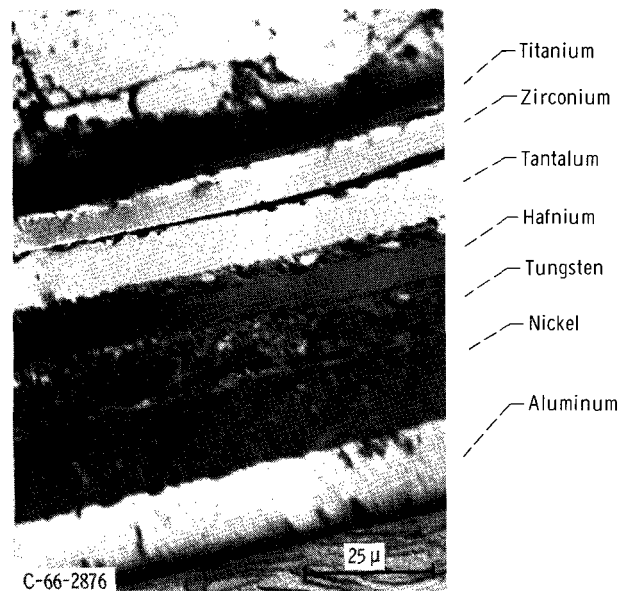


Figure 14. - SEEM photomicrograph of pressed laminate of titanium, zirconium, tantalum, hafnium, tungsten, nickel, and aluminum foils. Viewed at room temperature with 17.5-kilovolt nitrogen ions. X670.

clear separation between the two oxide dispersoids. Note that when air was used (fig. 13(c)) the general brightness level of the oxide particle images was higher than that obtained with the other two gases, but there was no apparent difference in brightness levels between the two oxides. The various micrographs in figure 13 are presented in the order in which the experiments were performed. Figures 13(a) and (d), both obtained with hydrogen ions, show that the same bombarding ion did not always give the same relative intensities of emission from oxide particles. Similar results (not pictured) were found in experiments where the specimen temperature and the discharge potential were independently varied (see table III, p. 12). None of the combinations of ion species, discharge potentials, and specimen temperatures used allowed unambiguous discrimination between these two oxides. Two phenomena were observed, which complicated interpretation when more than one of the oxide dispersoids was present. Although some operating conditions did produce a variation in particle brightness, the variation appeared as a continuous gradation rather than as distinct steps. An additional problem noted was that the brightness of individual particles alternately increased and decreased with time.

The micrograph of the foil laminate (fig. 14) illustrates the intensity difference between several metals under nitrogen ion bombardment. Note that there appear to be only two general levels of brightness. Zirconium, tantalum, and aluminum are much brighter than the other metals. Of interest is the fact that the hafnium foil has an intensity gradient. On the left side of the micrograph the intensity closely matches that of the adjacent tungsten foil. On the right side, however, the intensity of hafnium is definitely

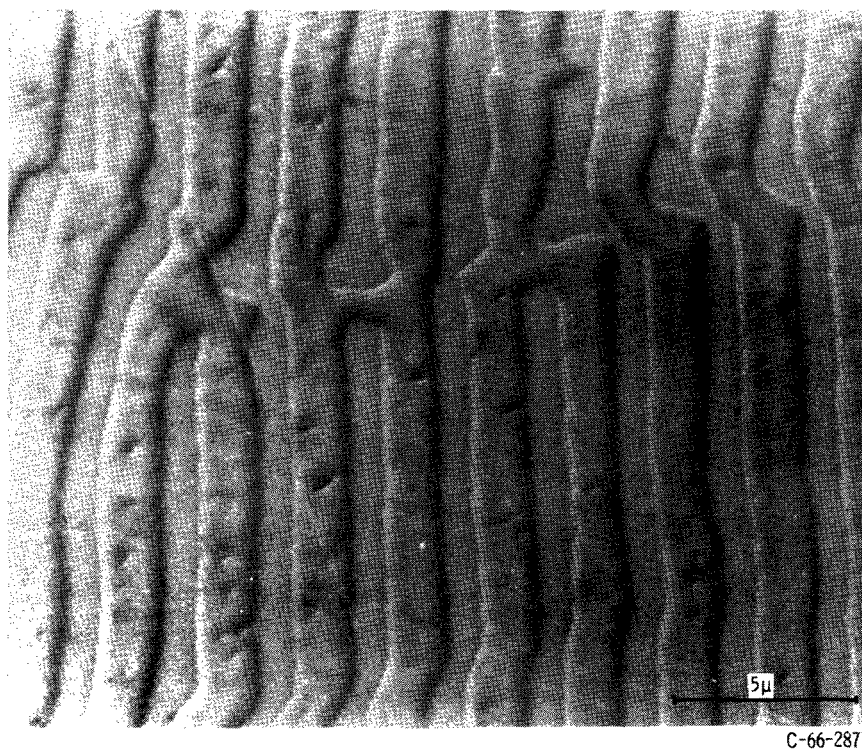


Figure 15. - SEEM photomicrograph of lamellae of unidirectionally solidified Al-CuAl₂ eutectic. Viewed at 80° C with 15-kilovolt nitrogen ions. X4700.

intermediate between the two general brightness levels.

A secondary emission micrograph of the lamellae of the Al-CuAl₂ eutectic (fig. 15) is an additional example of poor phase discrimination by intensity differences in an all-metal system. The image from the as-polished specimen initially showed no phase separation. Under ion bombardment the aluminum and CuAl₂ platelets were gradually revealed by preferential ion etching, and their separation was enhanced by using the shallowest angle of impingement of the ions. Here the phases are distinguished by their ion-etched topographies rather than by their brightness levels.

Other Practical Examples of Dispersion Microstructures

Viewed by SEEM and by CEM

Micrographs of a number of dispersion alloys of practical interest were taken with both the SEEM and the CEM. The alloys examined included dispersions of thorium and alumina in nickel, alumina in aluminum, thorium in tungsten, and zirconia in a tungsten-tantalum alloy.

Nickel-base alloys. - Figures 4(a) and (b) (p. 15) show the dispersion of thorium particles in TD-Nickel as observed in the SEEM and the CEM, respectively. Thorium particle

images are preferentially enlarged in the SEEM as noted in a previous section.

Figures 16 and 17 illustrate the use of the SEEM to examine compacted powder blend samples. Inspection of such samples can provide useful information for process control in the fabrication of dispersion alloys from powder. Figure 16(a) shows nickel powder with particle sizes of 1 to 2 microns blended with 1.4 volume percent of a much finer alumina, nominal particle size of 0.02 micron. These powders and proportions were purposely chosen to illustrate poor blending practice. The total surface area of the fine alumina was approximately equal to that of the nickel powder. Blending has resulted in an almost continuous network of alumina instead of a dispersion of discrete particles. Note that the alumina network, so clearly visible in the SEEM micrograph in figure 16(a), can hardly be distinguished in the CEM comparison micrograph in figure 16(b).

Better blending results are shown in figure 17(a), which is the SEEM micrograph of a blend of 8 volume percent alumina with nickel powder of comparable particle size, both being about 0.02 micron. Although individual particles are not resolved, the contrast between phases gives an indication of intimate blending and shows fair uniformity. There are some black areas, which can be interpreted as containing few if any alumina particles. Comparison micrographs taken in a CEM are shown in figures 17(b) and (c). The latter has had an annealing treatment to eliminate the matrix roughness, which interferes with observation of particles in figure 17(b).

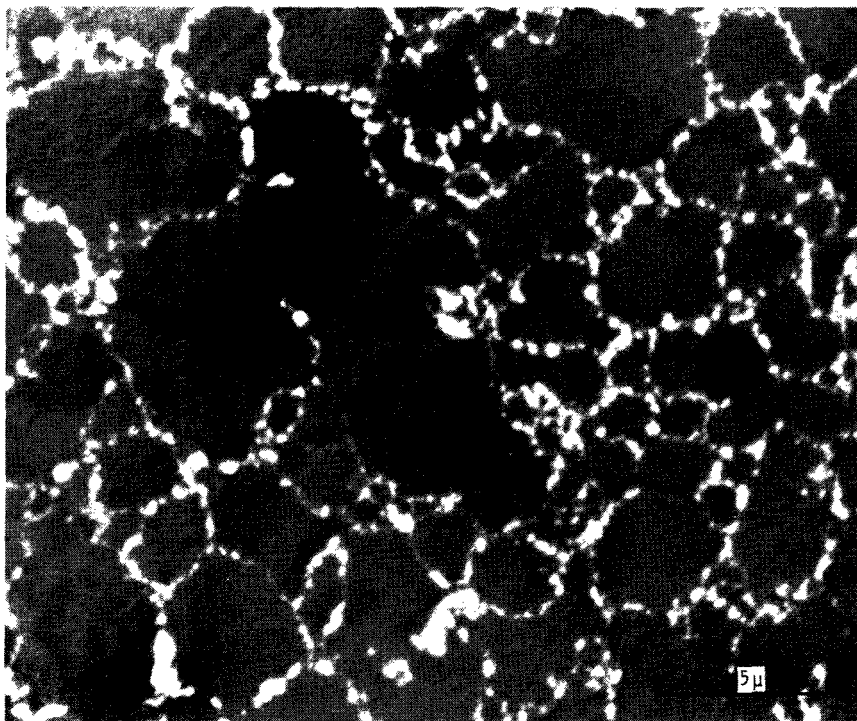
In the studies of compacted blends of nickel and alumina powders, it was noted that nickel oxide as well as alumina appeared as a bright phase in the SEEM. Figure 13 (pp. 32 and 33) illustrates the inconclusive results of experiments designed to differentiate two oxide phases.

Aluminum-base alloys. - A sample of M-257 alloy, aluminum plus 5 weight percent of alumina, was examined in both the SEEM and the CEM. Surprisingly, no bright oxide phase was observed in the polished condition in the SEEM. Subsequently, the specimen was chemically etched, as was done in the preparation for CEM replication, to give the result shown in figure 18(a) (p. 40), where particles are visible in relief but not by contrast. A much clearer distribution was observed in the CEM, as shown in figure 18(b).

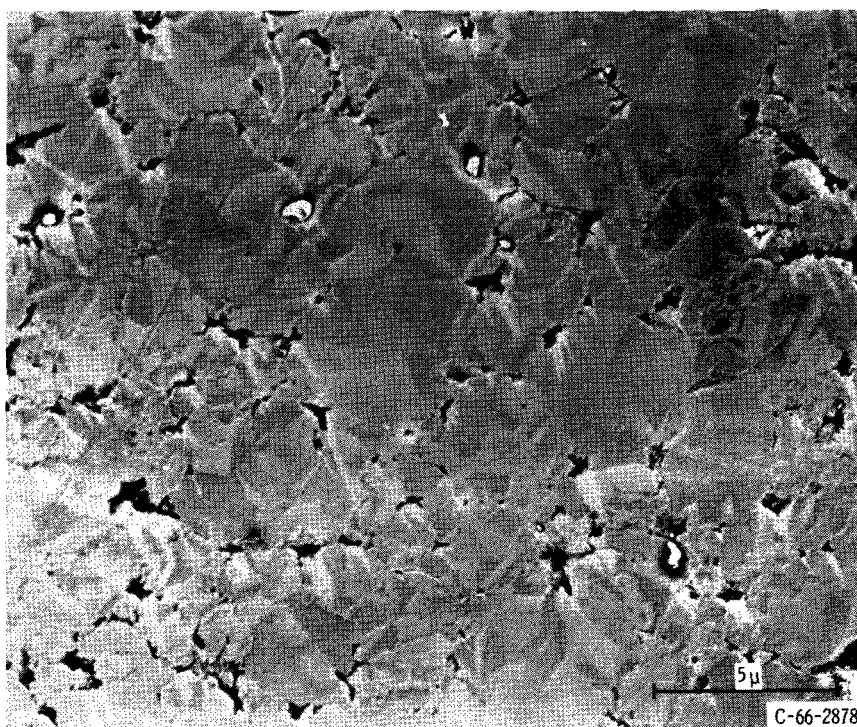
Tungsten-base alloys. - Three tungsten-base alloys were examined. Figure 9 (p. 27) shows a dispersion of coarse thoria particles with sizes up to 5 microns in a tungsten matrix. Note the high contrast that can be obtained when particles are well above the resolution limit of the SEEM.

A finer dispersion of thoria particles in a tungsten matrix is shown in figure 7 (p. 21). These micrographs were used to determine the dependence of the particle-image enlargement factor on particle size.

The third tungsten-base alloy examined had been fabricated from a blend of two powders: a tungsten-zirconium composite and a tantalum powder. The amount of zirconium present was 0.5 weight percent, and the amount of tantalum, 5 weight percent.

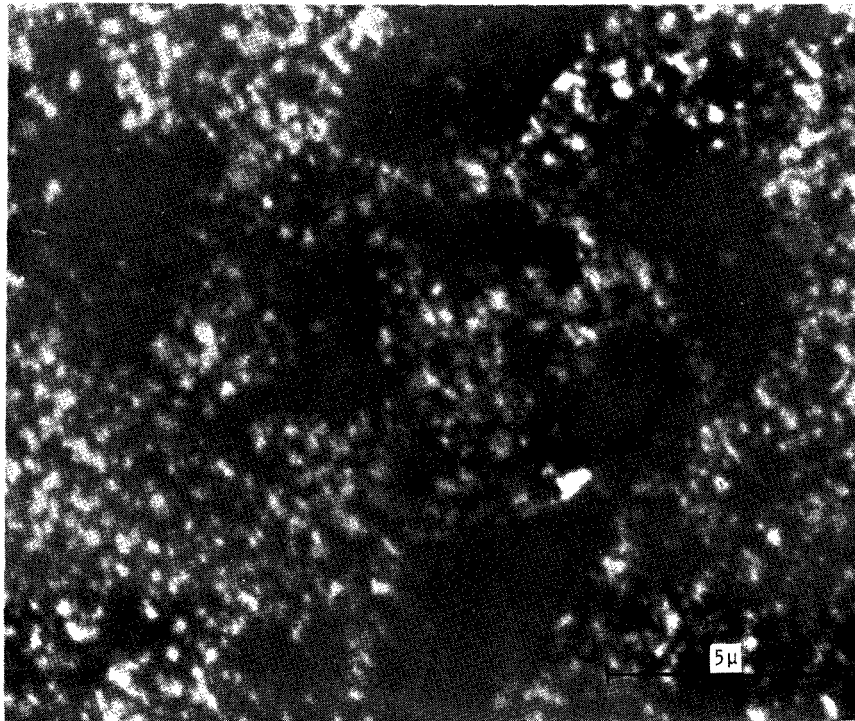


(a) As examined with SEEM. Viewed at 420° C with 17.5-kilovolt nitrogen ions.

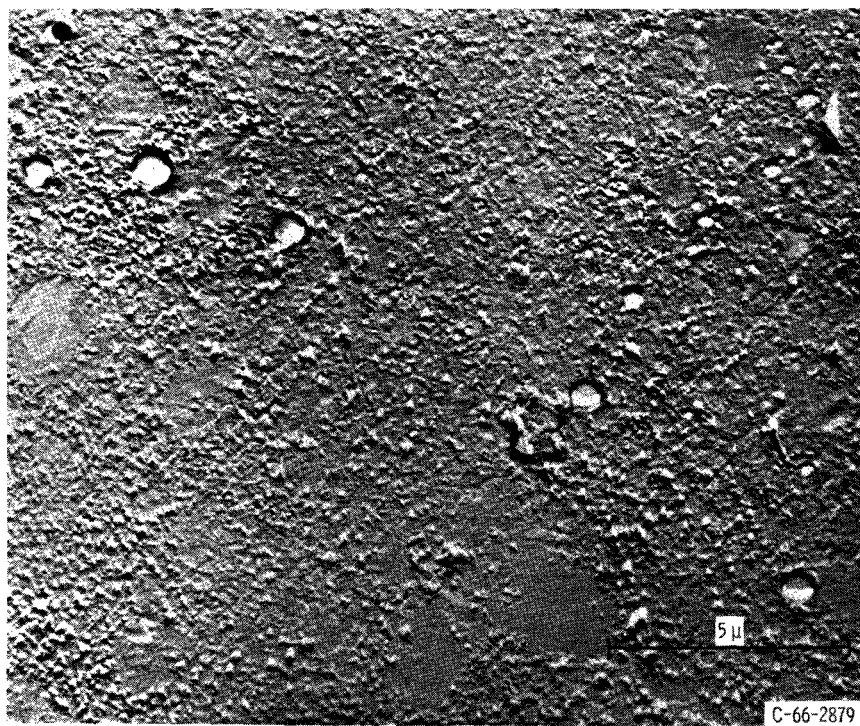


(b) As examined with CEM. Modified nickel etchant.

Figure 16. - Micrographs of explosively compacted, dry-blended alloy of nickel - 1.4 volume percent alumina. X4800.

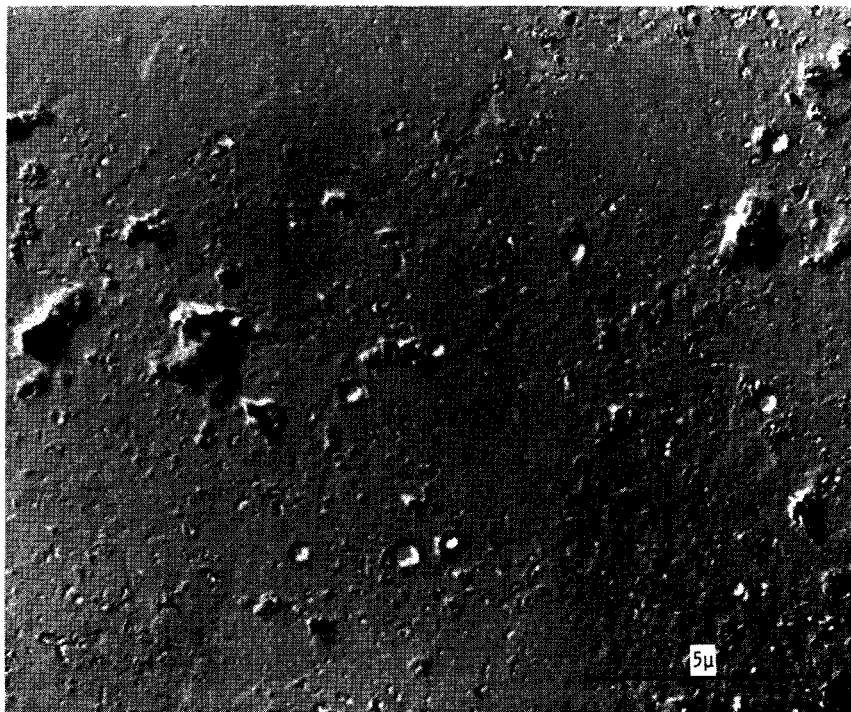


(a) As examined with SEEM. As compacted. Viewed at 415° C with 17.5-kilovolt nitrogen ions.

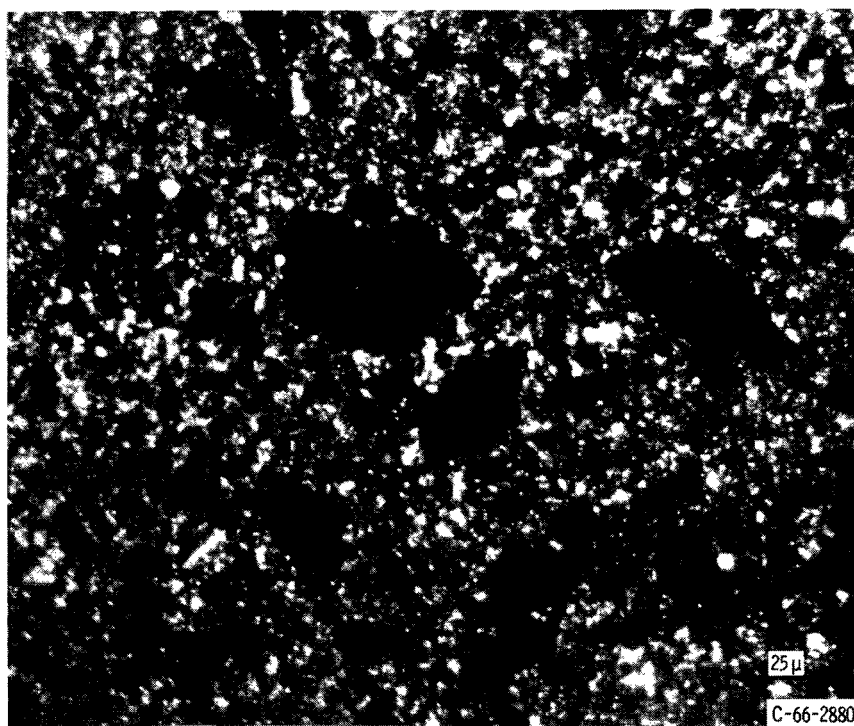


(b) As examined with CEM. As compacted. Modified nickel etchant. X6400.

Figure 17. - Micrographs of explosively compacted wet-blended alloy of nickel - 8 volume percent alumina alloy.

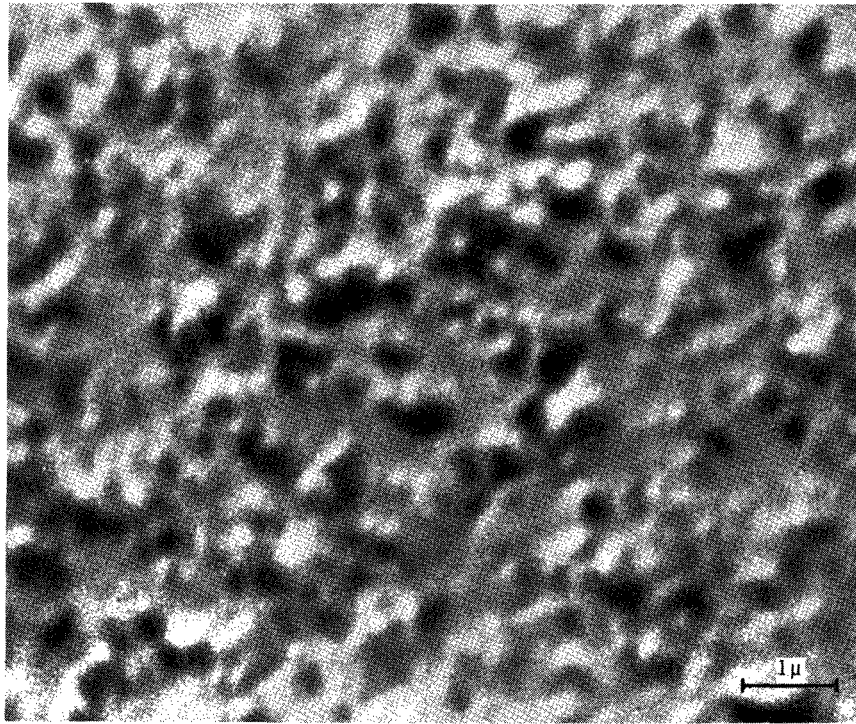


(c) As examined with CEM. As annealed. Modified nickel etchant. X6400.

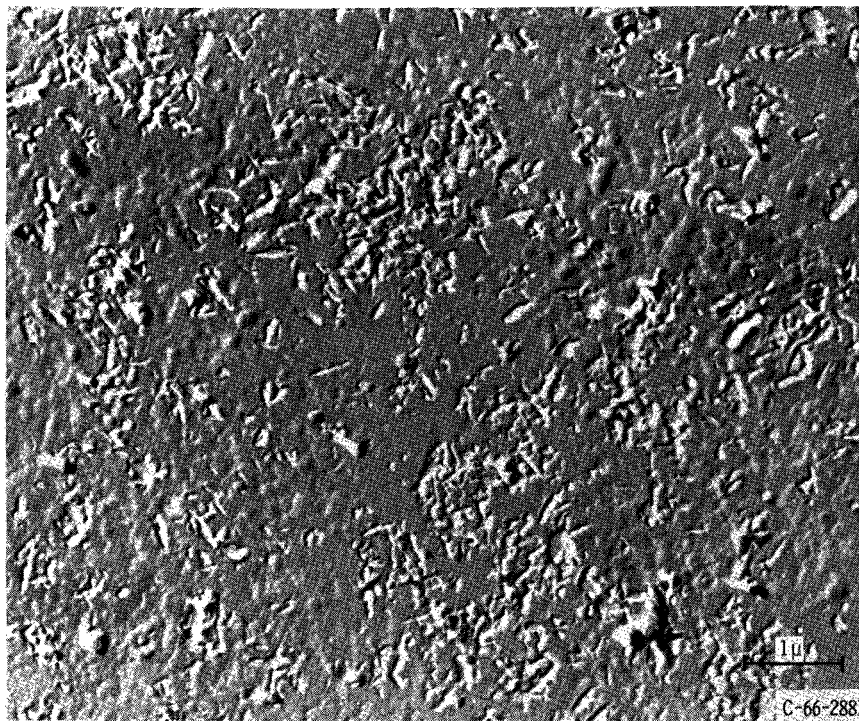


(d) As examined with optical microscope (dark field, polarized light). As compacted. X550.

Figure 17. - Concluded.

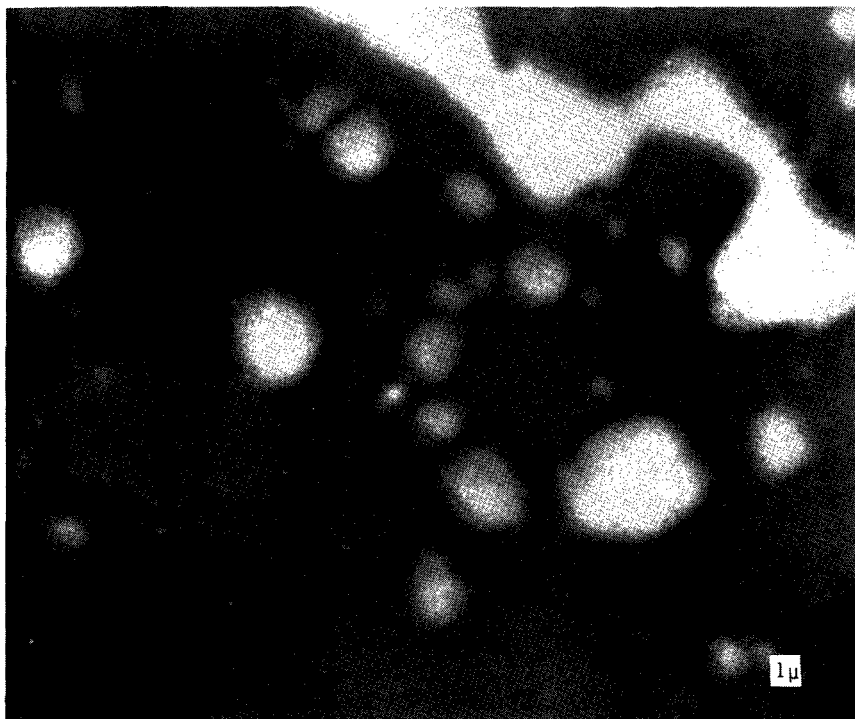


(a) As examined with SEEM. Chemically etched. Viewed at 390° C with 15-kilovolt nitrogen ions.

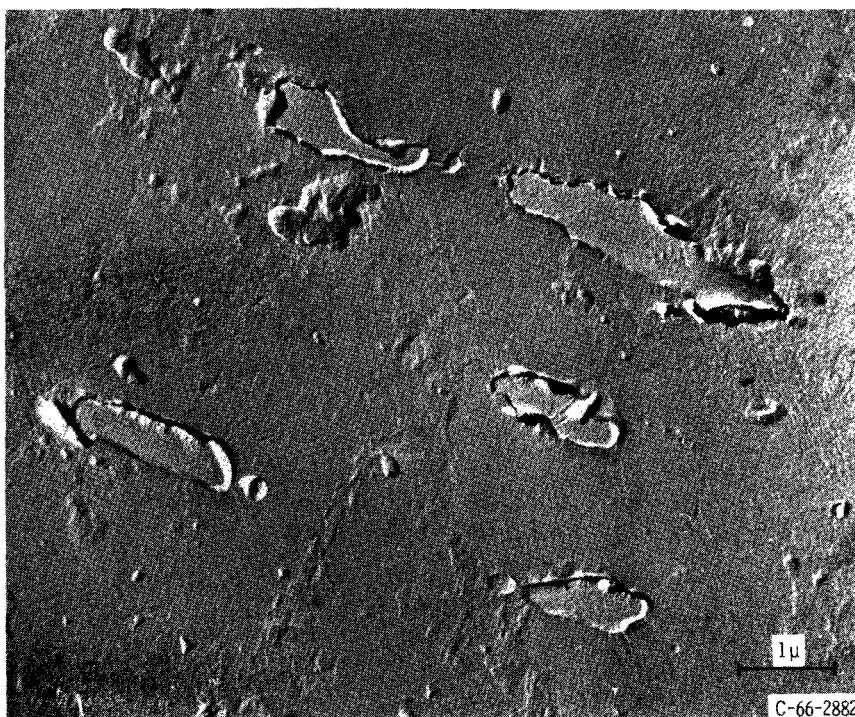


(b) As examined with CEM.

Figure 18. - Micrographs of extruded M-257 alloy (aluminum - 5 weight percent alumina). Transverse section. Modified sodium hydroxide etchant. X 12 000.



(a) As examined with SEEM. Viewed at 410° C with 15-kilovolt nitrogen ions.



(b) As examined with CEM. Etchant, 1 gram sodium hydroxide - 3.5 grams potassium ferricyanide - 50 milliliters water.

Figure 19. - Micrographs of extruded multiphase alloy of tungsten - 5 weight percent tantalum - 0.5 weight percent zirconium. Longitudinal section. X 12 000. •

Examination of this alloy in the polished condition in the SEEM revealed the mixture of large and small bright spots shown in figure 19(a). On the basis of the relative brightness levels of tungsten and tantalum established in the experiment with the foil laminate (fig. 14, p. 34), the large, bright regions in figure 19(a) were tentatively identified as tantalum-rich areas. Subsequent examination by a CEM using an etchant specific to tantalum (fig. 19(b)) and an electron beam microprobe verified these regions to be in fact tantalum rich. The smaller bright spots in figure 19(a) may be tantalum or zirconia particles.

DISCUSSION

The usefulness of secondary emission microscopy in the study of dispersion-strengthened metals depends on the extent to which an image of the surface can be obtained in which discrete phases can be distinguished and their true size and shape accurately measured. This report shows that for the examination of oxides dispersed in metals, great difficulty can be expected in obtaining precise values for microstructural parameters. This section discusses three aspects of the interpretation problem with secondary emission micrographs: resolution, image distortion, and phase discrimination.

Resolution and Detection Limits of SEEM

Although the theoretical resolution limit is about 80 Å (ref. 2), the working resolution of a secondary emission electron microscope of the type used in this study is generally stated by the manufacturer to be in the range 500 to 1000 Å.

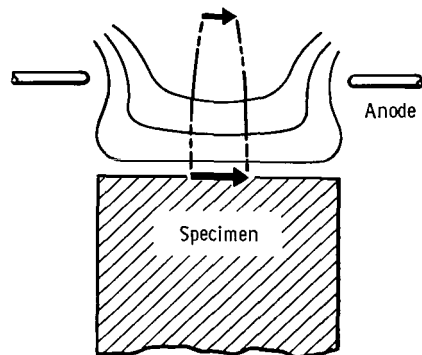
During the study of the phenomenon of particle image distortion, it became apparent that dispersion microstructures could be used to obtain an indirect measure of the resolution limit of the SEEM. By this indirect measurement, a value of 350 Å, which may be called a detection limit, was obtained for TD-Nickel.

That this value is more favorable than the 800-Å resolution limit determined in an all-metal system (fig. 3(a), p. 13) is attributed to two factors: the high contrast of the dispersoid-bearing microstructure and the preferential enlargement of the oxide particle images. The detection limit of the SEEM is about one-sixth of the resolution limit obtainable in a good light-optical system (2000 Å). Conventional electron microscopes, however, commonly have working resolution limits as low as 15 Å.

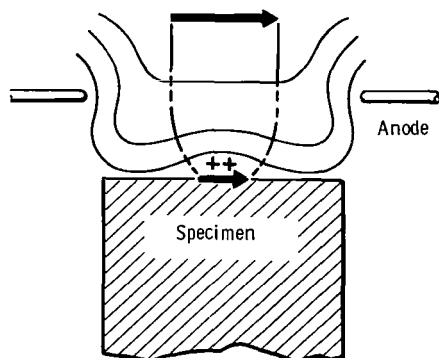
Distortion - Preferential Enlargement of Oxide-Particle Images

This study revealed that the images of fine oxide particles dispersed in metal matrices undergo preferential enlargement in the SEEM. The degree of this preferential enlargement, called the enlargement factor, has been shown to vary both with particle size and matrix composition. In the size ranges examined, the enlargement factors increased with particle size for thoria in nickel, whereas a decrease with particle size was measured for thoria particles in a tungsten matrix. Furthermore, the enlargement factor determined for a single coarse thoria particle in a second tungsten-thoria alloy did not agree with the trend of the data shown in table XI (p. 26) for an alloy of tungsten and fine thoria particles. Such complex distortion greatly complicates the use of the SEEM for quantitative metallography.

While no explanation for the irregularities in the measured enlargement factors is offered, it is suggested that the particle image exaggeration may be the result of a distortion in the electric field near the oxide particles in the specimen surface.



(a) Imaging of metal particle (represented by arrow).



(b) Imaging of oxide particle (represented by arrow).

Figure 20. - Schematic model of electric field near specimen surface in SEEM, illustrating possible source of image distortion with oxide particles.

Consider how this distortion might arise. In figure 20(a) the imaging of a discrete metal particle (represented by the arrow) in an all-metal specimen (cathode) is illustrated. The equipotential lines are smoothly curved, their configuration being determined by the field in the immersion objective. The lines of force, everywhere normal to the equipotential lines, image the metal particle at the focal point. If a nonconducting oxide particle lies in the specimen surface, the loss of electrons by emission can be supposed to leave a net positive charge on the particle. This may locally disturb the field at the surface (fig. 20(b)). In this case the lines of force would be deflected outward, and the resulting image size exaggerated. Each local distortion effectively acts as an additional lens in the electron optics.

Attempts at preventing charge buildup by vapor deposition of conducting film on the specimen were unsuccessful. Because of the low ion beam penetration, only a thin layer of a metal was necessary to obscure the microstructure of the specimen; however, the ion beam current required for the minimum image intensity necessary for focusing appar-

ently removed this conducting layer before observations could be made. The possibility that this problem could be avoided by a particular combination of ion gun species and vapor-deposited film should not be overlooked.

Charging of nonconductors has been observed previously in studies of polycrystalline alumina by secondary emission microscopy (refs. 3 and 9). The distortion appeared first only on certain grains and then in the center of the grain, the grain boundaries remaining undistorted. With time, this charging extended over the whole surface. This effect is surprising, however, with the dilute dispersions of very fine oxide particles where the high surface-to-volume ratio might be expected to allow the charge to be bled off to the conducting matrix.

Phase Discrimination

Three kinds of phase discrimination by the SEEM were examined in this study: discrimination between metals and oxides, between oxides and other oxides, and between metals and other metals. The high degree of phase contrast obtained for oxide particles dispersed in metal matrices has been shown in figures 4, 7, 9, and 16. Such high contrast and uniform intensity across individual particles (e.g., fig. 9, p. 27) could be ideally adapted to automatic scanning for purposes of quantitative metallography. Unfortunately, particle image distortion and the limited resolving power of the SEEM offset the advantage of high contrast.

Not all metal/oxide pairs exhibited high-phase contrast, however. Figure 18 (p. 40) shows alumina particles in aluminum with minimum dimensions of up to 0.180 micron. The larger particles are well above the detection limit of 0.035 micron determined for the SEEM, and yet they could not be detected by brightness difference alone. Possibly the lack of phase contrast was due to the presence of a film of aluminum oxide over the entire specimen.

Although the use of the SEEM for precise measurements of dispersion microstructures was found to be greatly hampered by limitations of the instrument, it might be considered as a tool for qualitative examination. For example, the differences between general fineness and uniformity of the dispersions in the compacted powder blends are readily seen (figs. 16 and 17, pp. 37, 38 and 39). In these cases, however, the SEEM results can be closely approached by light-optical results, although at somewhat lower magnifications. This is shown in figure 17(d), which is a photomicrograph taken with dark-field, polarized light and which corresponds to the SEEM image in figure 17(a).

As was previously pointed out, one of the difficulties in interpreting such dispersion micrographs is the problem of deciding whether all the bright phase observed is in fact the added dispersoid, or whether some of it may represent intrinsic oxide. Experiments

with two oxides in nickel indicated that phase discrimination between fine oxide particles in the size range near the resolution limit is unlikely to be achieved in the SEEM.

Brightness levels can often be used to discriminate between certain pairs of metals. With the exception of tantalum, the relative brightness levels of the foils in the foil composite of figure 14 (p. 34) were in accord with the relative secondary emission currents given in table I (p. 5). (Emission values for hafnium do not appear in table I.) The contrast between bright tantalum and dark tungsten was used to detect tantalum-rich areas in the microstructure shown in figure 19(a) (p. 41). That the areas were in fact rich in tantalum was subsequently confirmed by examination in an electron microprobe.

It is important to note, however, that there are potential applications of the SEEM outside the scope of this study where the various limitations discussed may not preclude successful use of the instrument. Examples of such applications include studies of solid-state phase transformations at elevated temperatures and qualitative aspects of oxidation and reduction phenomena (ref. 1).

CONCLUSIONS

Various operational aspects of a commercial secondary-emission electron microscope (SEEM) including the working resolution limit and the detection limit were determined. The application of this instrument to the examination of dispersion-strengthened materials was investigated. The principal conclusions can be summarized as follows:

1. Secondary-emission microscopy did not appear to be suitable for the quantitative examination of ultrafine oxide dispersions in metal matrices. The advantages of direct examination of an unetched specimen and high matrix/dispersoid contrast were offset by limited resolution and considerable distortion of the images of oxide particles.

2. The working resolution limit of the secondary-emission electron microscope used in this study was determined to be about 800 \AA (0.08μ); however, oxide dispersoid particles of true size as small as 350 \AA (0.035μ) can be detected in the instrument. This more favorable value is believed to result from high matrix/dispersoid contrast and preferential enlargement of oxide images.

3. Oxide particles dispersed in metals were imaged with linear dimensions enlarged as much as three times actual size. This resulted in an abnormally high apparent volume percent of dispersoid. This complex distortion not only precludes direct determination of microstructural parameters, but also apparently rules out simple correction schemes. The distortion is believed to be due to a charging of the nonconducting oxide particles, which magnifies their electron images.

4. Useful phase discrimination was evident when phases in the microstructure had substantially different secondary emission yields. This was true not only for oxide/metal

composites but was also demonstrated with a laminate of foils of several different metals. An attempt to discriminate between two oxides intermixed in a metal matrix was unsuccessful. Under certain conditions the SEEM may reveal phases observable only with great difficulty when conventional etching techniques are employed. Such phases are distinguished either by their different secondary electron emission characteristics or by a topographic separation resulting from their different rates of ion etching.

Lewis Research Center,
National Aeronautics and Space Administration,
Cleveland, Ohio, July 14, 1966,
129-03-01-05-22.

APPENDIX - QUALITATIVE EVIDENCE FOR IMAGE DISTORTION

The quantitative results are supported by qualitative evidence for an exaggeration of the oxide particle size when viewed in the SEEM. In all the micrographs obtained in this study, the images from oxide particles were not sharp. Although the metal matrix was often etched into sharply defined contours, the oxide particles appeared without any topographic detail. If the particles were imaged accurately, irregular oxide/matrix interfaces as observed in conventional electron microscopy would be visible (especially with the largest particles).

Additional insight into the distortion phenomenon came from observing the shadows of particles lying on the surface of the specimens. With insufficient washing of the polished specimen before examination or after a high-voltage discharge in the microscope during a run, oxide particles appeared resting on the surface. The shadows from these particles were invariably smaller than the particle image. The ratio of maximum shadow diameter to apparent particle diameter varied widely in a given specimen, which provided further evidence for a variable enlargement factor. Figures 11(a) to (c) (p. 29) illustrate the two types of shadows that were observed. With small alumina particles, shadows such as those in figures 11(a) and (b) were seen. The diameter of the shadow at its base is assumed to be approximately the true diameter of the particle. The length and shape of the shadow indicate the height and shape of the particle. With larger particles (fig. 11(c)), the shadow extends into the apparent particle area. This can be explained by assuming that the ion beam did not completely penetrate the particle and that no emission therefore occurred on the dark side. With smaller particles there is sufficient emission from the whole surface to restrict the shadow to the region outside the apparent area of the particle. Figure 11(d) is an example of a persistent distortion that appears occasionally in SEEM micrographs. It is not clear what causes this effect.

REFERENCES

1. Watts, R. D.: Surface Electron Microscopy. *Metallurgia*, vol. 66, no. 394, Aug. 1962, pp. 98-102.
2. Moellenstedt, G.: and Lenz, F.: Electron Emission Microscopy. Vol. 18 of *Advances in Electronics and Electron Physics*, L. Marton, ed., Academic Press, Inc., 1963, pp. 251-329.
3. Thornley, R. F. M.; and Cartz, L.: Direct Examination of Ceramic Surfaces with the Scanning Electron Microscope. *Am. Ceramic Soc. J.*, vol. 45, no. 9, Sept. 1962, pp. 425-428.
4. Bruining, H.: *Physics and Applications of Secondary Electron Emission*. Pergamon Press, 1954.
5. Kaminsky, Manfred: *Atomic and Ionic Impact Phenomena on Metal Surfaces*. Academic Press, 1965.
6. Gaukler, Karl H.: Messung der Elektronen-Emission im Metalloberflächenmikroskop. *Z. Metallk.*, vol. 51, 1960, pp. 463-466.
7. Reinhardt, Gustav; Cremens, Walter S.; and Weeton, John W.: Cold Consolidation of Metal plus Dispersoid Blends for Examination by Electron Microscopy. NASA TN D-3511, 1966.
8. Endter, F.; and Gebauer, H.: Ein einfaches Gerät zur statistischen Auswertung von mikroskopischen bzw. elektronenmikroskopischen Aufnahmen. *Optik*, vol. 13, no. 3, 1956, pp. 97-101.
9. Cartz, L.; Moellenstedt, G.; and Septier, A.: Emission Electron Microscope Studies of Ceramic Materials. *Transactions of the VIIIth International Ceramic Congress*, Copenhagen, 1962, pp. 21-28.

"The aeronautical and space activities of the United States shall be conducted so as to contribute . . . to the expansion of human knowledge of phenomena in the atmosphere and space. The Administration shall provide for the widest practicable and appropriate dissemination of information concerning its activities and the results thereof."

—NATIONAL AERONAUTICS AND SPACE ACT OF 1958

NASA SCIENTIFIC AND TECHNICAL PUBLICATIONS

TECHNICAL REPORTS: Scientific and technical information considered important, complete, and a lasting contribution to existing knowledge.

TECHNICAL NOTES: Information less broad in scope but nevertheless of importance as a contribution to existing knowledge.

TECHNICAL MEMORANDUMS: Information receiving limited distribution because of preliminary data, security classification, or other reasons.

CONTRACTOR REPORTS: Technical information generated in connection with a NASA contract or grant and released under NASA auspices.

TECHNICAL TRANSLATIONS: Information published in a foreign language considered to merit NASA distribution in English.

TECHNICAL REPRINTS: Information derived from NASA activities and initially published in the form of journal articles.

SPECIAL PUBLICATIONS: Information derived from or of value to NASA activities but not necessarily reporting the results of individual NASA-programmed scientific efforts. Publications include conference proceedings, monographs, data compilations, handbooks, sourcebooks, and special bibliographies.

Details on the availability of these publications may be obtained from:

SCIENTIFIC AND TECHNICAL INFORMATION DIVISION
NATIONAL AERONAUTICS AND SPACE ADMINISTRATION
Washington, D.C. 20546